Minibasin dynamics control sediment dispersal on a salt-detached slope: examples from the Northern Gulf of Mexico

Naiara Fernandez[1]*, Oliver B. Duffy[2], Frank Peel[2], Gillian Apps[2],

Christopher A.-L. Jackson[3], Michael R. Hudec[2]

[1]*Helmholtz Centre Potsdam, GFZ German Research Centre for Geosciences, Telegrafenberg, 14473 Potsdam, Germany*
[2]*Bureau of Economic Geology, Jackson School of Geosciences, The University of Texas at Austin, University Station, Box X, Austin, Texas, 78713-8924, USA*
[3]*Imperial College, Prince Consort Road, London, SW7 2BP, UK*

**Corresponding author: naiara@gfz-potsdam.de*

Minibasin dynamics control sediment dispersal on a salt-detached slope: examples from the Northern Gulf of Mexico

Naiara Fernandez[1]*, Oliver B. Duffy[2], Frank Peel[2], Gillian Apps[2],

Christopher A.-L. Jackson[3], Michael R. Hudec[2]

[1]Helmholtz Centre Potsdam, GFZ German Research Centre for Geosciences, Telegrafenberg, 14473 Potsdam, Germany
[2]Bureau of Economic Geology, Jackson School of Geosciences, The University of Texas at Austin, University Station, Box X, Austin, Texas, 78713-8924, USA
[3]Imperial College, Prince Consort Road, London, SW7 2BP, UK

**Corresponding author: naiara@gfz-potsdam.de*

Running Title: Minibasin dynamics control sediment dispersal

Keywords: salt tectonics; minibasins; Gulf of Mexico; salt-detached slopes; salt-sediment interaction; deep-water sediment transport; sediment dispersal

Abstract

Basal welds can halt the downslope translation of minibasins on salt-detached slopes, commonly giving rise to shortening and extension, updip and downdip, respectively, of the obstructed minibasins. How minibasin obstruction influences seafloor topography and thus deep-water sediment dispersal has not been previously investigated, despite it being an important control on hydrocarbon reservoir development. Using a 3D depth-migrated seismic reflection survey that images the mid-to-lower slope of the Northern Gulf of Mexico, we document: (1) minibasin welding and obstruction, and collision and overthrusting of an updip minibasin; and (2) extensional breakaway downdip of the welded minibasin. Using seismic attribute analysis, we show that these minibasin dynamics, controlled seabed relief and sediment dispersal. First, a slope-parallel submarine channel system was deflected perpendicular to the slope by relief generated by minibasin collision and overthrusting. A mass-transport complex (MTC) was subsequently deflected from its previous slope-parallel pathway by relief generated by uplift in the footwall of extensional breakaway-related normal fault. These results challenge traditional fill-and-spill models that consider only vertical subsidence and thus assume laterally static minibasins. Here, we highlight that minibasin mobility and obstruction exert an important influence on the seafloor morphology and hence, on the spatial configuration of deep-water depositional systems. Rather than a predictable response of the deep-water sediment transport system to minibasin obstruction related deformation, the obstruction-triggered seafloor topography changes are complex and locally constrained. Thus, we argue that a three-dimensional, dynamic salt-tectonic framework is required when assessing deep-water sediment dispersal on salt-influenced slopes where minibasin obstruction processes are ubiquitous.

Introduction

The distribution, geometry, and type of deep-water depositional systems are controlled by many factors (e.g., Rotzien et al., 2022). For example, at the regional-scale, tectonics and long-wavelength uplift and subsidence (e.g., Ingersol, 1990), as well as changes in relative sea level and sediment supply (Posamentier et al., 1988a, b), impact when, where, and how much sediment will reach the deep water. Upon reaching deep-water, seafloor topography, influenced by salt tectonics (e.g., Rowan and Weimer, 1998; Winkler and Booth, 2000; Mayall et al., 2000; Gee and Gawthorpe, 2006), faulting (e.g., Hodgson and Haughton, 2004), folding (e.g., Morley, 2007, 2009; Clark and Cartwright, 2009, 2012), or debris flow emplacement (e.g., Moscardelli and Wood, 2006, 2008; Armitage et al., 2009; Jackson and Johnson, 2009; Wu et al., 2020), then controls the local dispersal of sediment, and the type and distribution of relatively coarse-grained depositional systems, such as lobes and channels (Fig. 1a). Many of these topographic features are dynamic when considered in the context of the longevity of deposition (e.g., Jackson et al., 2021), meaning their increment growth can variably deflect or pond incoming sediments, thereby influencing their overall stratigraphic architecture (e.g., Mayall et al., 2000). This is especially the case in deep-water basins where salt is present, with the formation and subsidence of minibasins (see below) and related growth of adjacent diapirs, strongly and repeatedly modifying seafloor relief (e.g., Madof et al., 2009; Cumberpatch et al., 2021).

Minibasins are the main type of sedimentary depocenter formed on salt-detached slopes. When (temporarily) underfilled, minibasins provide accommodation that can be filled with coarse-grained sediments. When a minibasin is (temporarily) overfilled, the fill-and-spill model (*sensu* Prather et al., 1998) predicts that coarse-grained depositional systems, such as channels, will by-pass it and deliver sediment to downdip locations (e.g., Winker, 1996; Prather et al., 1998; Pirmez et al., 2000; Smith, 2004; Sinclair and Tomasso, 2002) (Fig. 1a). The classic fill-and-spill model assumes that depocenters remain undeformed and fixed in their horizontal position and that they are mobile only in the vertical direction. On salt-detached slopes, however, minibasins not only subside vertically into salt, but also translate horizontally, downslope, along with the flowing salt, for several tens of kilometres (e.g., Jackson et al., 2010; Pichel et al., 2018; Evans and Jackson, 2020; Fernandez et al., 2021; 2023). If the base-of-salt is not smooth and is instead characterized by variable relief, and if the translating minibasin is sufficiently thick, the minibasin can weld against base-salt and be obstructed from translating further downslope (Duffy et al., 2020). Salt and thinner (not-welded) minibasins can keep flowing around the obstructed minibasin. As a result, specific strain patterns can develop around the obstructed minibasin (Duffy et al., 2020; Fernandez et al., 2021; Fig. 1b). For example, an unwelded minibasin located downdip of the obstructed minibasin can pull away, forming an extensional breakaway zone (Fig. 1b). Similarly, an unwelded minibasin located updip of the obstructed minibasin can continue to move downslope, and converge towards the obstructed minibasin, driving shortening (Fig. 1b). If translation continues, the updip minibasin can weld against, or may even overthrust, the obstructed minibasin located further downslope (Duffy et al., 2020).

The northern Gulf of Mexico is an excellent example of salt-detached continental slope, which is also part of one of most prolific hydrocarbon provinces of the world (e.g., Weimer et al., 2017) (Fig. 2a). It is strongly influenced by salt-tectonic processes and populated with salt-withdrawal minibasins that are presently sinking into a thick salt canopy (Diegel et al., 1995, Pilcher et al., 2011) (Fig. 2b). In the northern Gulf of Mexico, minibasin obstruction and related complex strain patterns are widespread and well-documented (Krueger, 2010; Duffy et al., 2020; Fernandez et al., 2021). Precisely how minibasin dynamics due to their lateral translation, and specifically how obstruction processes impact the evolution of seafloor topography and the configuration of deep-water sedimentary systems, has not been yet investigated. In this study, we use high-quality 3D seismic reflection data to examine how minibasin obstruction can impact deep-water sediment dispersal patterns. We describe two examples of how minibasin obstruction in the study area has led to modification of syn-depositional seafloor relief and deep-water sediment dispersal.

Study Area and Dataset

The study area lies in the Northern Gulf of Mexico, encompassing part of the lower continental slope and the upper continental rise of offshore Louisiana (Fig. 2a). The continental slope overlies a thick allochthonous salt sheet (the Sigsbee Salt Canopy) (shown schematically on Fig. 1 and in seismic section on Fig. 2b). The Sigsbee Escarpment, at the downdip limit of the Sigsbee Canopy, is a major seafloor escarpment with km-scale relief and defines the boundary between the lower slope and the upper continental rise. The seafloor of the continental rise beyond the Sigsbee Escarpment is generally undeformed, with very low relief (Fig. 2a). The focus of this study is a set of minibasins that lie above the allochthonous salt of the Sigsbee Canopy. These supra-canopy minibasins have moved both vertically (subsiding into the salt) and laterally (downslope movement of the minibasins across the base of the canopy).

We use a 5219 km^2, 3D pre-stack, depth-migrated seismic reflection survey that images to a depth of 18 km. The seismic survey is owned by *WesternGeco Multiclient* and is commercially sensitive, so its precise location and orientation cannot be shown here; the general location is shown in Fig. 2a.

To preserve data vendor confidentiality, an unspecified but consistent reference direction is used throughout this paper on all maps and figures. For convenience, we label and refer to this reference direction as “North”. The precise rotation of our reference “North” direction to true geographic north is not specified here, however the true downslope direction is indicated on the figures. All maps and geospatial information derived from the data shown in this work have been rotated accordingly.

Methods

We used the 3D seismic data to map several key regional bounding surfaces; the sea floor, top of salt (Fig. 3a), and the base of the Sigsbee Salt allochthon (Fig. 3b), which we herein refer to as base-of-salt. We emphasize that this “base-of-salt” surface is not the base of autochthonous salt (Fig. 2b).

Seafloor and the top-of-salt define the top and bottom of the minibasins of interest and illustrates their geometry and distribution, while the base-of-salt defines the topography of the base of the Sigsbee canopy that influenced (and likely continues to influence) the salt-tectonic evolution of the slope and ultimately, the stratigraphic development of the minibasins (Fig. 3).

In addition to these structural bounding surfaces, we mapped several regional stratigraphic surfaces across both the continental rise (Fig. 4a) and the lower slope (Fig. 4b). Each of these regional surfaces correspond to a lateral shift in the position of the active sediment supply system. In the continental rise the mapped surfaces correspond to the condensed sequences that bracket the major submarine fan sequences (Fig. 4a). In the continental slope, the corresponding surfaces are expressed as onlap unconformities (Fig. 4b).

The Sigsbee Escarpment forms a major break between the suprasalt section on the slope and the equivalent age section on the continental rise, presenting a hurdle to correlation between the two domains. We approached this by mapping, for each sediment package on the slope, the sediment entry points onto to the Sigsbee Escarpment, and for each sediment package on the continental rise, the sediment entry out of the Escarpment, allowing us to match each internal on the slope with its equivalent on the continental rise.

All seismic stratigraphic horizons shown here within the minibasins on the slope are of Pleistocene age (Fig. 4). A provisional age assignment is shown in Table 1, which is based on well formation tops from data provided by the Gulf of Mexico Basin Depositional Synthesis (GBDS) industrial consortium database.

Root mean square (RMS) amplitude extractions were performed within a 50 m window centred on three of the regional horizons (dark-green, yellow and magenta horizons; Fig. 4, Table 1). Minibasin-scale RMS amplitude extractions were also performed at intermediate horizons in one of the minibasins. Following other studies of deep-water seismic geomorphology, high RMS values are interpreted to represent coarser, likely sand-rich sediment, whereas low RMS values likely reflect finer-grained deposits (e.g., Prather et al., 1998; Chopra and Marfurt, 2007). The RMS maps, in combination with seismic cross-sections, were used to map key depositional elements and erosional features, such as canyons, channels, lobes and mass transport complexes (MTC) (e.g., Prather et a., 1998).

Determining the magnitude and timing of minibasin-related faulting in the study area is important, given they document the pattern and extent of minibasin translation-related strain and therefore, the timing and likely impact on deep-water sedimentation. Fault throw (i.e., the difference between hangingwall and footwall cut-offs; e.g., Mansfield and Cartwright, 1996) was calculated for several seismic sections trending perpendicular to the local fault strike. The timing of salt-related faulting was assessed on similarly oriented profiles using expansion indices (EI) (i.e., the ratio of thickness between the layers in the hanging wall to those in the footwall; Thorsen, 1963; see also Jackson et al. 2017).

Present-Day Minibasin Configuration

The top-of-salt structure map illustrates the present-day configuration of the supra-canopy intra-slope minibasins, which vary in their shape and size (minibasins 1 through 5; Fig. 3a). Minibasin 1 is the most proximal, and is narrow (c. 7 km) and elongated in map-view, with its long-axis trending slope-parallel. Minibasins 2 and 3 are also elongated but wider (c. 12-14 km), with their long axis trending oblique to the slope. Minibasin 4 is also elongated and narrow, being the smallest minibasin in map-view. Minibasin 5 is the most distal minibasin imaged within the study area. It is elongated and relatively wide, and has a narrow, slope-perpendicular protrusion extending from its north-western margin (hereafter, referred to as the ‘neck’ of minibasin 5, Fig. 3a).

The base-of-salt (top of primary minibasins/base of salt canopy) and top-of-salt maps provide insights into the salt-tectonic development of the study area, in particular the likelihood that minibasins are welded, or whether they are still actively subsiding (Fig. 3a and b). The base-of-salt surface is irregular, with some marked topographic lows and highs. An area of low relief is found in the SW of the study area, below minibasin 1 and extending northwards as a linear trough. Another area of low relief is present in the central portion of the study area. Relatively flat and smooth base-of-salt highs separate these areas of low relief. Minibasins 4 and 5 are partially located over the base-of-salt lows and they are at present actively subsiding (Fig. 3b and 5). Instead, minibasins 2 and 3 are located predominantly above base-of-salt topographic highs and are welded at their base (Fig. 3b and 6). However, whereas the main body of minibasin 5 is located over a base-of-salt low, its north-western neck extends over a base-of-salt high where it is partially welded (Fig. 3b and 7).

Given that minibasins 2 and 3 in the study area are welded whereas the other minibasins are still subsiding, we expect complex patterns of intra- and inter-minibasin strain due to minibasin obstruction. We now focus on two case studies in which minibasin obstruction has led to shortening and extension: 1) minibasin obstruction and updip collision and overthrusting; and 2) minibasin obstruction and downdip extensional breakaway. For both cases, we also document the configuration of the deep-water depositional systems before and after the onset of obstruction-induced deformation.

Case 1: Minibasin Collision and Overthrusting causes Channel Diversion

Example of minibasin obstruction and updip shortening

Minibasin 5 is only welded below its north-westerly neck (Figs. 3b and 7). Partial welding of minibasin 5 occurs because the base-of-salt is shallower directly below its north-westerly neck (Fig. 3b). In contrast to minibasin 5, the minibasin immediately updip, minibasin 4, is not welded, and sits within still-thick salt (Fig. 5 and 7). Directly updip of the main part of minibasin 5, minibasins 4 and 5 are separated by a diapir (Fig. 5). Conversely, directly updip of the north-westerly welded neck of minibasin 5, minibasin 4 over-thrusts minibasin 5 (Fig. 7).

We interpret this configuration between minibasins 4 and 5, arises because the north-westerly neck of minibasin 5 is welded and obstructed (*sensu* Duffy et al., 2021) and therefore impeded from further downslope translation, whereas updip minibasin 4 can still translate downslope, leading to collision between and overthrusting of minibasin 4 onto minibasin 5 (Fig. 8). Critically, stratigraphic onlap onto the upslope-dipping limb of the syncline defining minibasin 4 is most pronounced between the dark-green and yellow horizons (Fig. 5 and 7). We interpret that this onlapping sequence documents the onset of minibasin collision, shortening, and thrusting. The equivalent stratigraphic package in minibasin 5 is slightly wedge-shaped, thickening towards the overthursted edge of the depocenter (Fig. 7). We interpret this local thickening to record minibasin subsidence and tilting caused by loading of minibasin 4 onto the SW flank of minibasin 5 (Fig. 8). The presence of seafloor relief and underfilled accommodation in minibasin 5 suggests shortening between minibasins 4 and 5 is still ongoing (Fig. 7).

Channel system configuration before minibasin collision

We now describe the configuration of the sediment transport system in the study area at the time of the dark-green horizon (Fig. 4b), which we interpret to be *before* the collision of minibasins 4 and 5 and thrusting of the former over the latter. Seismic data indicate the presence of a channel system within an c. 800 m-thick, Pleistocene unit within minibasin 2 (yellow polygon in Fig. 4b). The channel system is characterized by at least three, laterally-to-vertically stacked, erosionally based channels, which are 800 m to 3 km-wide and up to 200 m-deep (Fig. 4b). The channels contain variable-amplitude, continuous to discontinuous seismic reflections, encased within predominantly low and moderate-to-high amplitude, continuous to semi-discontinuous reflections. Attribute analysis of the dark-green horizon and observation from seismic cross-sections show several areas of high amplitude which appear to be aligned to form a curvilinear feature (i.e., in minibasin 1 and 3, and outboard of the canopy; Fig. 9a). Based on its relatively high amplitude, which we interpret to represent relatively coarse-grained sediments (i.e., sandy), its curvilinear channel-like form, and its dimensions and morphology, we interpret this linear feature as a submarine channel system (e.g., Posamentier and Kolla, 2003), incised into low-to-moderate amplitude, likely mudstone-dominated slope sediments. The channel system trends broadly ENE-WSW (i.e., broadly perpendicular to the shelf edge), passing from minibasin 1 to minibasin 2, and ultimately south-westwards into minibasin 5, before exiting the area of seismic mapping at the edge of the present-day salt canopy, extending onto the continental rise (Fig. 9a). At the continental rise, the submarine channel system takes a bend, first turning slightly to the left and then to the right.

Channel system configuration after minibasin collision

The RMS amplitude extraction along the younger yellow horizon (Fig. 9b), which we interpret to be after the onset of collision and overthrusting between minibasins 4 and 5, shows a similar linear channel-like morphology in map-view (Fig. 9b). Based on its high-amplitude expression, we also interpret this feature is a coarse-grained channel-system and to be incised into finer-grained, potentially muddy slope sediments. Updip, the channel system has a similar trend to the underlying, older channel system (i.e., it trends broadly ENE, passing between minibasins 1, 2 and 5; green and yellow circles in Fig. 9a, b). However, further downslope, the channel displays a 90º bend at the updip margin of minibasin 5, such that it trends NW (Fig. 9b), parallel to the canopy edge, passing through the north-westerly neck of minibasin 5, before bending to trend N and exiting the canopy onto the continental rise. As such, the new canopy-edge spill-point of the younger channel system is located c. 20 km NW of the older spill-point (i.e., the yellow star in Fig. 9b).

Sediment transport system captured by minibasin overthrusting

We have described the general change in the configuration of the channel system before and after the onset of the collision and overthrusting of minibasin 4 onto minibasin 5 (Fig. 9a and b). We now use four higher-resolution RMS amplitude extractions within minibasin 5 (from the regional dark-green and yellow horizons, which document the pre- and post-collision morphology, respectively) to help unravel the sequence of events associated with this change (Fig. 10a):

Step 1 - Pre-thrusting channelized deposition (dark-green horizon equivalent). The slope-parallel submarine channel system, which here it is ~5 km wide, was present. The channel system crossed minibasin 5 and exited via the downdip spill point of Step 1 (Fig. 10a).

Step 2 - Pre-thrusting depositional hiatus. The lack of high-amplitudes suggests that at this time, coarse-grained sediments were not being deposited in minibasin 5, which was instead characterized by the deposition fine-grained slope sediments (Fig. 10a).

Step 3 -Thrusting, and MTC emplacement and ponding. Two different seismic facies are observed in two distinct areas (Fig.10a): a) an area (c. 15 km^2) of relatively low-to-moderate amplitude, chaotic seismic reflections, occupying the western central portion of minibasin 5, adjacent to the boundary with minibasin 4; this is interpreted as an mass-transport complex (MTC) locally sourced from gravitational collapse of the footwall of the thrust defining the overthrusted boundary between minibasins 4 and 5 (e.g., Moscardelli and Wood, 2006; 2008); and b) a localized area of relatively high amplitude in the southwest portion of the minibasin; we interpret this as an area of ponded, coarse-grained sediment, possibly within a frontally confined lobe (e.g., Prather et al., 1998, Posamentier and Kolla 2003).

Step 4 - Syn-thrusting deposition (yellow horizon equivalent). A narrower (1-2 km), curvilinear belt of high amplitudes is observed at the southwest portion of the minibasin, which we interpret as the re-established channel system (Fig. 10a). The channel system takes a sharp turn to the left, parallel to the edge of the minibasin. Although the channel system cannot be directly followed across the north-westerly neck of minibasin 5, based on the regional RMS extraction (Fig. 9b) we infer that the spill point is at the canopy-edge, c. 20 km NW of its location during Step 2.

In summary, after the onset of minibasin collision and shortening-induced thrusting, the channel system was re-established with a new configuration, following a new course across minibasin 5, parallel to that of the growing thrust defining the updip margin of the depocenter. We interpret that this new channel pathway arose in response to the new topographic configuration at the north-westerly edge of minibasin 5, i.e., overthrusting of minibasin 4 onto minibasin 5 would have tilted the neck of minibasin 5, generating accommodation, as recorded by the wedge-shaped sediment package we observe in this location, and capturing the channel system (Fig. 10b).-

Case 2: Minibasin Extensional Breakaway deflects an MTC

Example of minibasin obstruction and downdip extension

We now assess another example of minibasin obstruction dynamics in the study area, in this case related to obstruction of minibasin 2 and the related development downdip minibasins 3 and 5 (Figs 3, 6 and 11). Minibasins 2 and 3 are both welded at their base (Fig. 6). The main body of minibasin 5, however, located directly downdip of minibasin 2, is not welded (Fig. 11). This means the main body of minibasin 5 is still able to subside and translate downslope. We interpret that the obstruction of minibasin 2 on base-of-salt relief, and the ongoing translation of the main body of downslope minibasin 5, caused the formation of an extensional breakaway (*sensu* Duffy et al., 2021) (Fig. 12), expressed by the development of normal fault systems and related grabens between minibasin 2 and downdip minibasins 3, 4 and 5 (Fig. 13a). However, to assess whether the extensional deformation in the area is the result of the welding and obstruction of minibasins 2 and 3 we need to understand the timing of welding and related faulting.

Minibasin 3 was most probably welded well-before the time of the dark-green horizon. The timing of welding is indicated by the turtle structure and flank depocenters (i.e., rim synclines) below the dark-green horizon in minibasin 3 (Fig. 6). The axial trace of the turtle structure within minibasin 3 indicates the stacking of centrally located, bowl-like depocenters before the minibasin welded at its base. Basal welding below this central depocenter caused the subsequent shifting of depocenters towards the flanks of minibasin 3 (forming the turtle structure and rim synclines), which was followed by the deposition of aggradational, isopachous sequences in the minibasins, which started earlier than the dark-green horizon (Fig. 6 and 11). Equivalent isopachous sequences are also observed in minibasin 2 below the dark-green horizon, again indicating welding of minibasin 2 occurred before the time of the dark-green horizon (Fig. 11).

Having determined when the minibasins welded, we now assess the timing of faulting. A detailed analysis of the expansion index of the fault segments between minibasins 2, 3 and 5, indicates they were active at different times (Fig. 13a). For example, the faults were inactive before the welding of minibasins 2 and 3 (Fig. 13a). The most downdip fault segment F1 (between minibasins 3 and 5) then became active, during the dark-green time interval, after and we infer, in response to the welding of minibasins 2 and 3. Strain subsequently migrated updip through the fault system, initially to fault F2, with deformation finally reaching the area between minibasin 2 and minibasins 4 and 5 at the time of light-green and magenta intervals, when segment F3 probably formed (Fig. 13a).

The observed fault kinematics are consistent with variations in the timing, magnitude, and spatial pattern of salt-canopy advance across the continental rise (i.e., down-dip), as determined by plotting the landward cutoffs of the different stratigraphic levels on the continental rise stratigraphy below the salt (e.g., Hudec and Jackson, 2006) (Fig. 13b). More specifically, in front of the welded minibasin 3, the cutoffs are tightly-spaced in map-view, indicating limited horizontal advance of canopy edge. In contrast, there is an important period of canopy advance in front of minibasin 5 between the dark-green horizon and the magenta horizon (Fig. 13b). Critically, not only is the magnitude of canopy advance and extension strain accommodated by the breakaway extensional system are comparable (i.e., c. 1.5 km), but the timing is also similar (i.e., between the light-green horizon and the yellow horizon).

MTC configuration after minibasin obstruction and extensional breakaway

We now assess the configuration of the sediment transport system in the study area at the time of the magenta horizon, when the fault F3 had already formed (Fig. 13). We want to understand if, and how, the sediment transport system was influenced by the obstruction of minibasins 2 and 3 and formation of the associated extensional breakaway. In minibasins 2 and 3, the amplitude map is dominated by a several-km-wide, linear features of relatively low-to-moderate amplitude, and which exhibits notable, edge-parallel lineaments and some chaotic reflections (Fig. 9c). We interpret this as a mass transport complex (MTC), with the lineaments representing erosive scours carved by the source flow as it travelled downslope (e.g., Moscardelli and Wood, 2006; 2008). The MTC is c. 100 m-thick in minibasin 2 and has an area extent of at least c. 190 km^2 (Fig. 4b). In the updip portion of the study area, the MTC reuses the same pathway as the older channel system (i.e., it extends from minibasin 1 to minibasin 2; Fig. 9c). However, instead of following a straight, slope-parallel path towards minibasin 5, like the earlier channel systems, the MTC turns sharply right and then left, and trends East towards minibasin 3 (Fig. 9c).

MTC deflected by a topographic barrier

The earlier submarine channel system imaged within the yellow horizon trended broadly slope-parallel, passing from minibasin 2 into minibasin 5 (Fig. 9b). Only the fault F1, located between minibasin 3 and 5, was active at the time of the deposition of the yellow horizon (Fig. 13b). It was not until the time after this time and before the deposition of the magenta horizon that the fault F2, developed on the pathway between minibasins 2 and 5 (Fig. 13b).

In a slope-parallel seismic profile, oriented parallel to the channel system between minibasins 2 to 5, we can see that the faults are affecting the seafloor, with extension mainly accommodated by the landward-dipping fault segment F2 (Fig. 14a). The downslope footwall of the fault forms a topographic high, possibly enhanced by the flow of salt from below minibasin 5, which is still subsiding, into the diapir between minibasins 2 and 5 (Fig. 5 and 14). We interpret that similar or greater relief may have been present at the time of deposition of magenta horizon, generating a barrier to the downslope transport of the MTC (Fig. 14c). As a result, the MTC was not able to travel from minibasin 2 to minibasin 5 like the earlier channel system, but instead it had to circumvent the topographic barrier (Fig. 8c, 14b).

Discussion

In classic fill-and-spill models (*sensu* Prather et al., 1998), a minibasin keeps ponding coarse-grained sediment until overfilled, at which time the sediment transport system can bypass the now-filled minibasin and deposit coarse-grained sediment downslope (e.g., Sinclair and Tomasso, 2002; Prather et al., 1998; Prather, 2000; 2003; Smith, 2004). The fill-and-spill model assumes that accommodation in minibasins is controlled by the steady-state slope profile, and that minibasin slope profiles are static. In contrast to this predominantly two-dimensional and static view of salt-sediment interactions, many studies have now tried to capture the more three-dimensional aspects of the fill-and-spill model in areas of salt tectonics, where it has been documented that channel systems can be diverted by salt-tectonic influenced seabed relief, resulting in complex sediment transport pathways and resultant stratigraphic architectures (e.g., Hay, 2012; Madof et al., 2009; 2017; Mayall et al., 2010). The patterns of accommodation development within individual minibasins can also vary in response to welding and/or tilting of minibasins prior to welding (e.g., Fernandez et al., 2020; Jackson et al., 2021; Duffy et al., 2021).

However, even in these works addressing the three-dimensional, the time-varying nature of salt-sediment interactions and the potential impact of lateral mobility of minibasins (translation vs. obstruction) on deep-water sediment dispersal was not acknowledged.

Complex deformation processes associated with (laterally) mobile and/or obstructed minibasins have been previously documented in the northern Gulf of Mexico (e.g., Krueger, 2005; Duffy et al., 2020; 2021; Fernandez et al., 2021). In this study, we have provided two new examples of this type of minibasin interaction: a) minibasin obstruction and updip minibasin collision and overthrusting; and b) minibasin obstruction and formation of a downdip extensional breakaway. One key observation from our study is that rather than being either fully obstructed or fully mobile, individual minibasins can be partially obstructed and partially mobile (i.e., minibasin 5; Fig. 3). As such, along-strike of a minibasin margin, strain may pass from extensional to contractional (Fig. 14b).

Duffy et al. (2020) anticipated that minibasin obstruction processes would lead to predictable changes in the seafloor topography, thus potentially controlling the location and character of deep-water depositional systems. However, the specific ways in which minibasin obstruction is reflected on the seafloor topography and changes in deep-water sediment dispersal has not previously been documented in detail. Shortening structures (e.g., folds and thrust) are most frequently expressed as positive relief features on the seafloor topography of salt-detached slopes (e.g., Morley, 2009); this is the case for the shortening structure delineating the updip margin of obstructed minibasin 5 in our study area, with positive relief defined by the thrust hanging-wall itself (Fig. 7). Shortening-induced loading also drives tilting and accommodation development in footwall of the updip thrust (Fig. 7). Conversely, extensional deformation on salt-detached slopes is often accommodated by the formation of normal fault-bounded graben-like depocenters (e.g., Oppo et al., 2024; see also the area above the diapir between minibasins 2 and 3; Fig. 6). However, the extensional breakaway (*sensu* Duffy et al. 2020) that formed downdip of obstructed minibasin 2 is also associated with a local bathymetric high (Fig. 14a), partly associated with footwall uplift adjacent to salt-detached faults, but principally due to salt-flow and reactive diapirism (Fig. 12).

Submarine channel systems and MTCs are strongly influenced by sea-floor topography. Positive relief caused by shortening structures or diapirs are in most of the cases thought of as potential barriers to sediment dispersal (Fig. 1) (e.g., Morley, 2009). In this study, however, the first change in channel-related sediment dispersal (dark-green to yellow horizons) was caused by overthrusting of minibasin 4 onto 5, which rather than acting as a topographic barrier, triggered the capture of a channel system due to the loading and tilting of the partially obstructed minibasin 5 (Fig. 15a, b). By contrast, the negative relief formed during extensional breakaway-related normal faulting is typically anticipated to help channelize or capture deep-water flows (e.g., Oppo et al., 2024). However, in this study, local fault- and salt flow-driven uplift creates a topographic high, leading to channelization rather than deflection of an MTC (Fig. 15b, c). These two examples of minibasin obstruction-related deformation support the prediction of Duffy et al. (2020) that these dynamics exert an important influence on the seafloor morphology and hence, the spatial configuration of deep-water depositional systems. However, the arising salt-sediment interactions vary over short length scales and are rather complex.

It is notable that the updip and downdip portions of the deep-water depositional systems behave differently through the studied time span. While in the updip portion of the study area the sediment transport system reuses a well-established pathway through minibasins 1 and 2, the downdip portion undergoes two main pathway reconfigurations (Fig. 15). Given the relatively limited spatial extent of the study area, the source area of the submarine channel system and MTC cannot be observed, and we can only speculate on the reasons for this downdip change in behaviour. Whether a submarine channel system or MTC will be able to overcome (e.g., bypass or erode) a topographic barrier depends, at least in part, on the energy of the flow transporting the sediments and the height of the topographic barrier on its pathway (e.g., Kneller and McCaffrey, 1999). Considering this, it is noted that the turbidite currents that most probably formed the submarine channel system and the subsequent debris flow that emplaced the MTC would differ in how they respond to topographic relief due to their distinct rheologies (i.e., they act as Newtonian and non-Newtonian fluids respectively; Gani, 2004). Regardless of the specific differences between the submarine channel system and the MTC, one reason of why we observe pathway reconfigurations only in downslope locations, might be that the flows transporting the sediments lost some of their energy as their travelled downslope, making them slower and more prone to be affected by changes in seafloor topography. An alternative hypothesis may be that in the relatively downslope, toe-of-slope position, close to the edge of the salt-canopy where the base-of-salt gets shallower (Fig. 2 and 3), minibasins are more likely to weld and undergo obstruction-related dynamics.

Conclusions

We have used a 3D pre-stack, depth-migrated seismic reflection survey to study a cluster of supra-salt minibasins located in the mid-to-lower slope of the Northern Gulf of Mexico. We have mapped several horizons that are correlated across the different minibasins, three of which are regionally correlated across the continental rise, outboard of the salt canopy. We have provided two new examples of minibasin obstruction processes and have described in detail the observed deformation patterns around the obstructed minibasins, i.e., updip shortening accommodated by minibasin collision and overthrust and downdip extensional deformation accommodated by an extensional breakaway.

We have used seismic attribute interpretation (RMS amplitude) on the three regional horizons to map the nature and pathway configuration of the sediment transport systems across the cluster of minibasins in the study area. Although the updip portion of the sediment transport system remains unchanged, we have observed and described two main shifts in the pathway configuration of the sediment transport system in the downdip portion of study area: 1) a submarine channel system that gets rerouted with respect to an earlier configuration, and 2) a mass-transport complex (MTC) that gets deflected with respect to the earlier submarine channel system pathway.

Based on the available observations from the seismic data, we have been able to interpret these two shifts in the depositional system as responses to changes on the seafloor topography caused by minibasin obstruction processes. Our study documents for the first time how salt-tectonic processes related to minibasin obstruction can modify the slope seafloor topography and control deep-water sediment dispersal. We have been able to illustrate how the zones of shortening updip of obstructed minibasins do not simply act as potential persistent seafloor topographic barriers to downslope sediment transport, and that normal-fault bounded grabens do not necessarily aid channelized flow as is usually implied in simplified conceptual models of the fill-and-spill model. Thus, rather than a predictable response of the deep-water sediment transport system to obstruction related deformation, the obstruction-triggered seafloor topography changes are locally constrained and complex. Furthermore, our study showcases that individual minibasins can be partially obstructed and partially mobile, implying that strain along a minibasin margin can shift from extensional to contractional. We thus argue that a more three-dimensional, detailed, dynamic salt-tectonic framework is required when assessing deep-water sediment dispersal on salt-influenced slopes.

Although our study has focused on supra-canopy minibasins in the northern Gulf of Mexico, the findings are broadly applicable to any salt-detached slope where the minibasin mobility and lateral translation are influenced by the base-of-salt topography or by interactions with nearby minibasins. Since sediment dispersal patterns are closely tied to reservoir distribution and properties, the processes outlined above are relevant for exploration in salt-bearing sedimentary basins.

Acknowledgements

WesternGeco Multiclient is acknowledged for providing the 3D seismic data and for giving permission to publish the results of this research. PaleoScan and Decision Space were used under the corresponding academic agreements between Eliis and The University of Texas at Austin and between Halliburton and The University of Texas at Austin. Dallas Dunlap is acknowledged for his assistance in the RMS extraction workflow in Eliis. We thank the Gulf Basin Depositional Synthesis (GBDS) Industrial Associates Program at The University of Texas at Austin for access to their database. This work was funded by the Applied Geodynamic Laboratory (AGL) Industrial Associates Program at the University of Texas at Austin (the updated list of associated companies can be checked here: www.beg.utexas.edu/agl/sponsors). During the execution of this study, the authors received additional support from the Jackson School of Geosciences at The University of Texas at Austin.

Table 1. List of mapped regional structural and stratigraphic horizons, with provisional age assignment.

Name	Biostrat., Datum	Structural Significance	Epoch	Age (stage)	Age (ma)
Seafloor	n/a	Top of minibasins	Holocene	-	0
Magenta	-	Intra minibasin	Pleistocene	Greenlandian?	-
Yellow	*Trim. A*	Intra minibasin	Pleistocene	Top Calabrian	0.74
Dark-green	*Ang. B*	Intra minibasin	Pleistocene	Intra Calabrian	1.54
Top of Salt	n/a	Bottom of minibasins	Variable	Variable	n/a
Base of Salt	n/a	Bottom of Sigsbee Canopy	Variable	Variable	n/a

References

Anderson, J.E., Cartwright, J., Drysdall, S.J. and Vivian, N., 2000. Controls on turbidite sand deposition during gravity-driven extension of a passive margin: examples from Miocene sediments in Block 4, Angola. Marine and Petroleum Geology, 17(10), pp.1165-1203. https://doi.org/10.1016/S0264-8172(00)00059-3

Armitage, D.A., Romans, B.W., Covault, J.A. and Graham, S.A., 2009. The influence of mass-transport-deposit surface topography on the evolution of turbidite architecture: The Sierra Contreras, Tres Pasos Formation (Cretaceous), southern Chile. *Journal of Sedimentary Research*, *79*(5), pp.287-301. https://doi.org/10.2110/jsr.2009.035

Booth, J.R., Dean, M.C., DuVernay III, A.E. and Styzen, M.J., 2003. Paleo-bathymetric controls on the stratigraphic architecture and reservoir development of confined fans in the Auger Basin: central Gulf of Mexico slope. Marine and Petroleum Geology, 20(6-8), pp.563-586. https://doi.org/10.1016/j.marpetgeo.2003.03.008

Chopra, S. and Marfurt, K.J., 2007. Seismic attributes for prospect identification and reservoir characterization. Society of Exploration Geophysicists and European Association of Geoscientists and Engineers. 481 pp. https://doi.org/10.1190/1.9781560801900.ch1

Clark, I.R. and Cartwright, J.A., 2009. Interactions between submarine channel systems and deformation in deepwater fold belts: Examples from the Levant Basin, Eastern Mediterranean Sea. Marine and Petroleum Geology, 26(8), pp.1465-1482. https://doi.org/10.1016/j.marpetgeo.2009.05.004

Clark, I.R. and Cartwright, J.A., 2012. Interactions between coeval sedimentation and deformation from the Niger delta deepwater fold belt. In "Application of the Principles of Seismic Geomorphology to Continental Slope and Base-of-Slope Systems: Case Studies from SeaFloor and Near-Sea Floor Analogues" edited by Prather, Deptuck, Mohrig, Van Hoorn, and Wynn https://doi.org/10.2110/pec.12.99.0243

Cumberpatch, Z.A., Kane, I.A., Soutter, E.L., Hodgson, D.M., Jackson, C.L., Kilhams, B.A. and Poprawski, Y., 2021. Interactions between deep-water gravity flows and active salt tectonics. Journal of Sedimentary Research, 91(1), pp.34-65. https://doi.org/10.2110/jsr.2020.047

Diegel, F.A., Karlo, J.F., Schuster, D.C., Shoup, R.1. and Tauvers, P.R., 1995. Cenozoic structural evolution and tectono-stratigraphic framework of the northern Gulf Coast continental margin. In “Salt Tectonics: A Global Perspective” edited by M.P.A. Jackson, D.G. Roberts, S. Snelson. https://doi.org/10.1306/M65604C6

Duffy, O.B., Fernandez, N., Peel, F.J., Hudec, M.R., Dooley, T.P. and Jackson, C.A.L., 2020. Obstructed minibasins on a salt-detached slope: An example from above the Sigsbee canopy, northern Gulf of Mexico. Basin Research, 32(3), pp.505-524. https://doi.org/10.1111/bre.12380

Duffy, O.B., Dooley, T.P., Hudec, M.R., Fernandez, N., Jackson, C.A.L. and Soto, J.I., 2021. Principles of shortening in salt basins containing isolated minibasins. Basin Research, 33(3), pp.2089-2117. https://doi.org/10.1111/bre.12550

Fernandez, N., Hudec, M.R., Jackson, C.A.L., Dooley, T.P. and Duffy, O.B., 2020. The competition for salt and kinematic interactions between minibasins during density-driven subsidence: observations from numerical models. *Petroleum Geoscience*, *26*(1), pp.3-15. https://doi.org/10.1144/petgeo2019-051

Fernandez, N., Duffy, O.B., Peel, F.J. and Hudec, M.R., 2021. Influence of minibasin obstruction on canopy dynamics in the northern Gulf of Mexico. Basin Research, 33(1), pp.427-446. https://doi.org/10.1111/bre.12480

Fernandez, N., Duffy, O., Jackson, C., Kaus, B., Dooley, T., & Hudec, M. (2023). How Fast Can Minibasins Translate Down a Slope? Observations from 2D Numerical Models. *τeκτonıκa*, *1*(2), 177–197. https://doi.org/10.55575/tektonika2023.1.2.22

Galloway, W.E., 1975. Process framework for describing the morphologic and stratigraphic evolution of deltaic depositional systems. In “Deltas: Models for Exploration”, Houston Geological Society.

Gani, M.R., 2004. From turbid to lucid: a straightforward approach to sediment gravity flows and their deposits. *The Sedimentary Record*, *2* (3), pp.4-8. https://doi.org/10.2110/sedred.2004.3.4

Gee, M.J.R. and Gawthorpe, R.L., 2006. Submarine channels controlled by salt tectonics: Examples from 3D seismic data offshore Angola. Marine and Petroleum Geology, 23(4), pp.443-458. https://doi.org/10.1016/j.marpetgeo.2006.01.002

Hodgson, D.M. and Haughton, P.D., 2004. Impact of syndepositional faulting on gravity current behaviour and deep-water stratigraphy: Tabernas-Sorbas Basin, SE Spain. Geological

Society, London, Special Publications, 222(1), pp.135-158. https://doi.org/10.1144/GSL.SP.2004.222.01.08
Howlett, D.M., Gawthorpe, R.L., Ge, Z., Rotevatn, A. and Jackson, C.A.L., 2021. Turbidites, topography and tectonics: Evolution of submarine channel-lobe systems in the salt-influenced Kwanza Basin, offshore Angola. Basin Research, 33(2), pp.1076-1110. https://doi.org/10.1111/bre.12506
Hudec, M.R. and Jackson, M.P., 2006. Advance of allochthonous salt sheets in passive margins and orogens. *AAPG bulletin*, *90*(10), pp.1535-1564. https://doi.org/10.1306/05080605143
Ingersoll, R.V., 1990. Tectonics of sedimentary basins. Geological Society of America Bulletin, 100(11), pp.1704-1719. https://doi.org/10.1130/SPE253-p57
Jackson, M.P.A., Hudec, M.R. and Dooley, T.P., 2010. Some emerging concepts in salt tectonics in the deepwater Gulf of Mexico: intrusive plumes, canopy-margin thrusts, minibasin triggers and allochthonous fragments. In *Geological Society, London, Petroleum Geology Conference series* (Vol. 7, No. 1, pp. 899-912). London: The Geological Society of London. https://doi.org/10.1144/0070899
Jackson, C.A.L., Duffy, O.B., Fernandez, N., Dooley, T.P., Hudec, M.R., Jackson, M.P. and Burg, G., 2020. The stratigraphic record of minibasin subsidence, Precaspian Basin, Kazakhstan. *Basin Research*, *32*(4), pp.739-763. https://doi.org/10.1111/bre.12393
Jackson, C.A. and Johnson, H.D., 2009. Sustained turbidity currents and their interaction with debrite-related topography; Labuan Island, offshore NW Borneo, Malaysia. *Sedimentary Geology*, *219*(1-4), pp.77-96. https://doi.org/10.1016/j.sedgeo.2009.04.008
Jackson, C.A., McAndrew, A.E., Hodgson, D.M. and Dreyer, T., 2021. Repeated degradation and progradation of a submarine slope over geological timescales. Journal of Sedimentary Research, 91(1), pp.116-145. https://doi.org/10.2110/jsr.2020.77
Kneller, B. and McCaffrey, W., (1999), Depositional effects of flow nonuniformity and stratification within turbidity currents approaching a bounding slope; deflection, reflection, and facies variation. *Journal of Sedimentary Research*, 69 (5): 980–991. https://doi.org/10.2110/jsr.69.980
Krueger, S., (2010). Dynamics of tear faults in the salt-detached systems of the Gulf of Mexico [abs.], in. Proceedings AAPG Annual Convention & Exhibition Abstracts, 19, 137–138.

Loncke, L., Gaullier, V., Mascle, J., Vendeville, B. and Camera, L., 2006. The Nile deep-sea fan: an example of interacting sedimentation, salt tectonics, and inherited subsalt paleotopographic features. Marine and Petroleum Geology, 23(3), pp.297-315. https://doi.org/10.1016/j.marpetgeo.2006.01.001

Madof, A.S., Christie-Blick, N. and Anders, M.H., 2009. Stratigraphic controls on a salt-withdrawal intraslope minibasin, north-central Green Canyon, Gulf of Mexico: Implications for misinterpreting sea level change. AAPG bulletin, 93(4), pp.535-561. https://doi.org/10.1306/12220808082

Madof, A.S., Christie-Blick, N., Anders, M.H. and Febo, L.A., 2017. Unreciprocated sedimentation along a mud-dominated continental margin, Gulf of Mexico, USA: Implications for sequence stratigraphy in muddy settings devoid of depositional sequences. *Marine and Petroleum Geology*, *80*, pp.492-516. https://doi.org/10.1016/j.marpetgeo.2016.12.022

Mansfield, C.S. and Cartwright, J.A., 1996. High resolution fault displacement mapping from three-dimensional seismic data: evidence for dip linkage during fault growth. Journal of Structural Geology, 18(2-3), pp.249-263. https://doi.org/10.1016/S0191-8141(96)80048-4

Mayall, M., Lonergan, L., Bowman, A., James, S., Mills, K., Primmer, T., Pope, D., Rogers, L. and Skeene, R., 2010. The response of turbidite slope channels to growth-induced seabed topography. AAPG bulletin, 94(7), pp.1011-1030. https://doi.org/10.1306/01051009117

Morley, C.K., 2007. Interaction between critical wedge geometry and sediment supply in a deep-water fold belt. Geology, 35(2), pp.139-142. https://doi.org/10.1130/G22921A.1

Morley, C.K., 2009. Growth of folds in a deep-water setting. Geosphere, 5(2), pp.59-89. https://doi.org/10.1130/GES00186.1

Moscardelli, L. and Wood, L., 2008. New classification system for mass transport complexes in offshore Trinidad. *Basin research*, *20*(1), pp.73-98. https://doi.org/10.1111/j.1365-2117.2007.00340.x

Moscardelli, L., Wood, L. and Mann, P., 2006. Mass-transport complexes and associated processes in the offshore area of Trinidad and Venezuela. *AAPG bulletin*, *90*(7), pp.1059-1088. https://doi.org/10.1306/02210605052

Oluboyo, A.P., Gawthorpe, R.L., Bakke, K. and Hadler-Jacobsen, F., 2014. Salt tectonic controls on deep-water turbidite depositional systems: Miocene, southwestern Lower Congo Basin, offshore Angola. Basin Research, 26(4), pp.597-620. https://doi.org/10.1111/bre.12051

Oppo, D., Jackson, C.A.L. and Maselli, V., 2024. Early extensional salt tectonics controls deep-water sediment dispersal. https://doi.org/10.1130/B37786.1

Pirmez, C., Beaubouef, R.T., Friedmann, S.J. and Mohrig, D.C., 2000. Equilibrium profile and baselevel in submarine channels: examples from Late Pleistocene systems and implications for the architecture of deepwater reservoirs. In "Deep-Water Reservoirs of the World" edited by Paul Weimer. https://doi.org/10.5724/gcs.00.15.0782

Posamentier, H.W., Jervey, M.T. and Vail, P.R., 1988. Eustatic controls on clastic deposition I—conceptual framework. In "Sea-Level Changes: An Integrated Approach" edited by Cheryl K. Wilgus, Bruce S. Hastings, Henry Posamentier, John Van Wagoner, Charles A. Ross, Christopher G. St. C. Kendall. https://doi.org/10.2110/pec.88.01.0109

Posamentier, H.W. and Vail, P.R., 1988. Eustatic controls on clastic deposition II—sequence and systems tract models. In "Sea-Level Changes: An Integrated Approach" edited by Cheryl K. Wilgus, Bruce S. Hastings, Henry Posamentier, John Van Wagoner, Charles A. Ross, Christopher G. St. C. Kendall. https://doi.org/10.2110/pec.88.01.0125

Posamentier, H.W. and Kolla, V., 2003. Seismic geomorphology and stratigraphy of depositional elements in deep-water settings. *Journal of sedimentary research*, *73*(3), pp.367-388. https://doi.org/10.1306/111302730367

Prather, B.E., Booth, J.R., Steffens, G.S. and Craig, P.A., 1998. Classification, lithologic calibration, and stratigraphic succession of seismic facies of intraslope basins, deep-water Gulf of Mexico. AAPG bulletin, 82(5), pp.701-728. https://doi.org/10.1306/1D9BC5D9-172D-11D7-8645000102C1865D

Prather, B.E., 2003. Controls on reservoir distribution, architecture and stratigraphic trapping in slope settings. Marine and Petroleum Geology, 20(6-8), pp.529-545. https://doi.org/10.1016/j.marpetgeo.2003.03.009

Prather, B.E., 2000. Calibration and visualization of depositional process models for above-grade slopes: a case study from the Gulf of Mexico. Marine and Petroleum Geology, 17(5), pp.619-638. https://doi.org/10.1016/S0264-8172(00)00015-5

Rotzien, J.R., Caldwell, R.L. and Goggin, L.R., 2022. Deepwater depositional environments. In Deepwater Sedimentary Systems (pp. 251-300). Elsevier. https://doi.org/10.1016/C2021-0-00094-8

Rowan, M.G. and Weimer, P., 1998. Salt-sediment interaction, northern Green Canyon and Ewing bank (offshore Louisiana), northern Gulf of Mexico. AAPG bulletin, 82(5), pp.1055-1082.

Sinclair, H.D. and Tomasso, M., 2002. Depositional evolution of confined turbidite basins. Journal of Sedimentary Research, 72(4), pp.451-456. https://doi.org/10.1306/111501720451

Smith, R.U., 2004. Silled sub-basins to connected tortuous corridors: sediment distribution systems on topographically complex sub-aqueous slopes. In "Confined Turbidite Systems", edited by S. A. Lomas, P. Joseph. https://doi.org/10.1144/GSL.SP.2004.222.01.03

Thorsen, C.E., 1963. Age of growth faulting in southeast Louisiana. Trans. Gulf Coast Assoc. Geol. Soc. 13, 103-110.

Weimer, P., Bouroullec, R., Adson, J. and Cossey, S.P., 2017. An overview of the petroleum systems of the northern deep-water Gulf of Mexico. AAPG Bulletin, 101(7), pp.941-993. https://doi.org/10.1306/09011608136

Winker, C.D. and Booth, J.R., 2000. Sedimentary dynamics of the salt-dominated continental slope, Gulf of Mexico: integration of observations from the seafloor, near-surface, and deep subsurface. In "Deep-Water Reservoirs of the World", edited by Paul Weimer. https://doi.org/10.5724/gcs.00.15.1059

Wu, N., Jackson, C.A.L., Johnson, H.D., Hodgson, D.M. and Nugraha, H.D., 2020. Mass-transport complexes (MTCs) document subsidence patterns in a northern Gulf of Mexico salt minibasin. Basin Research, 32(6), pp.1300-1327. https://publons.com/publon/10.1111/bre.12429

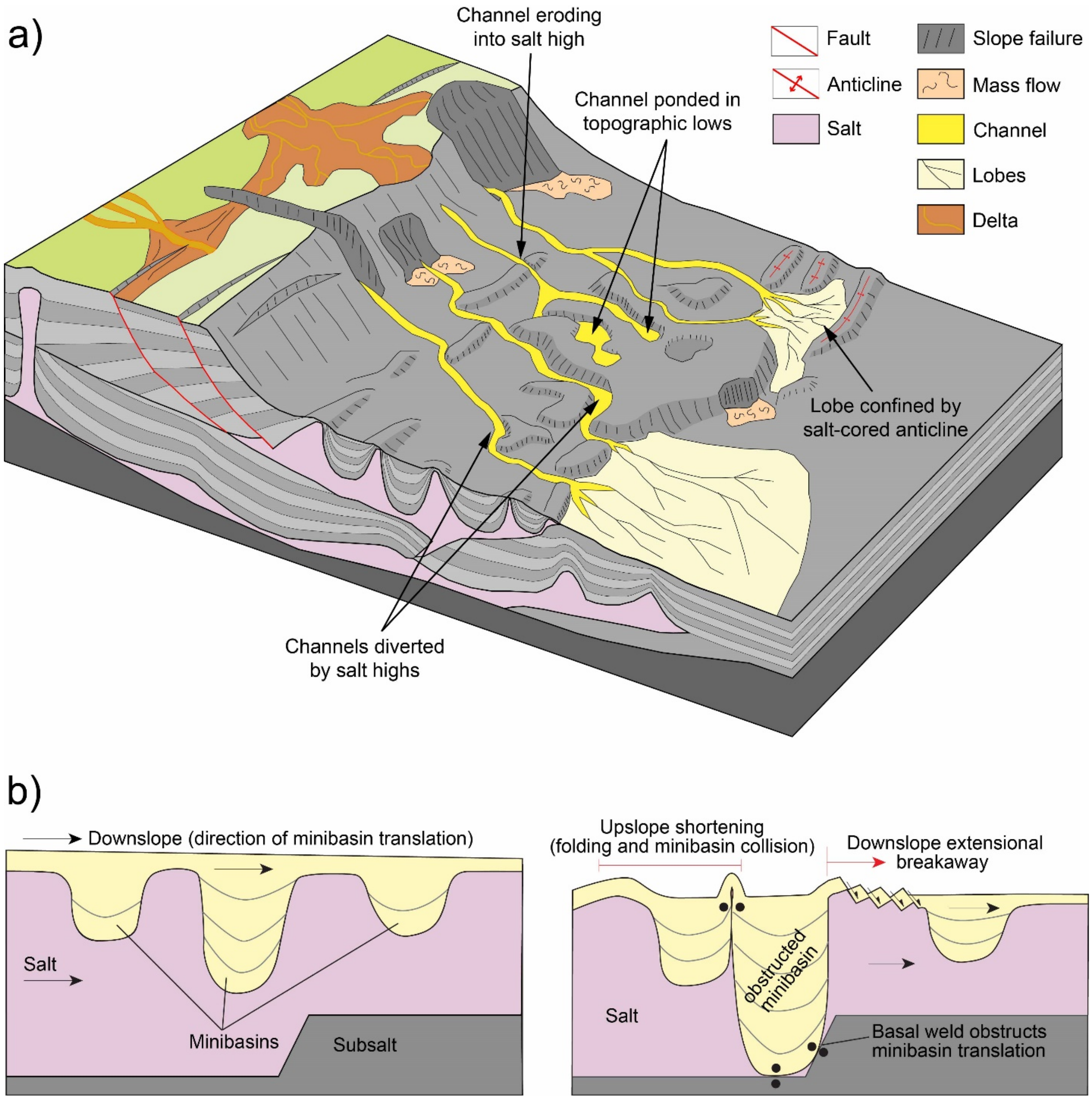

Figure 1. ***a)*** *Schematic illustration of a continental slope from shelf to slope-floor, where the structural controls on deep-water depositional systems are summarized (after Mayall et al., 2010, and Cumperpatch et al., 2021). Note that several interactions between the channels-lobes and seafloor topography (modified by salt structures) are highlighted.* ***b)*** *Schematic diagram showing the concept of minibasin obstruction on an area with high relief base-salt. At an early the thin minibasins are translating downslope. At a later stage, central minibasin is thick enough to weld against base-salt, and is obstructed. Minibasin obstruction creates a zone of shortening updip of obstructed minibasins, and a zone of extension downdip of obstructed minibasin (after Duffy et al., 2020).*

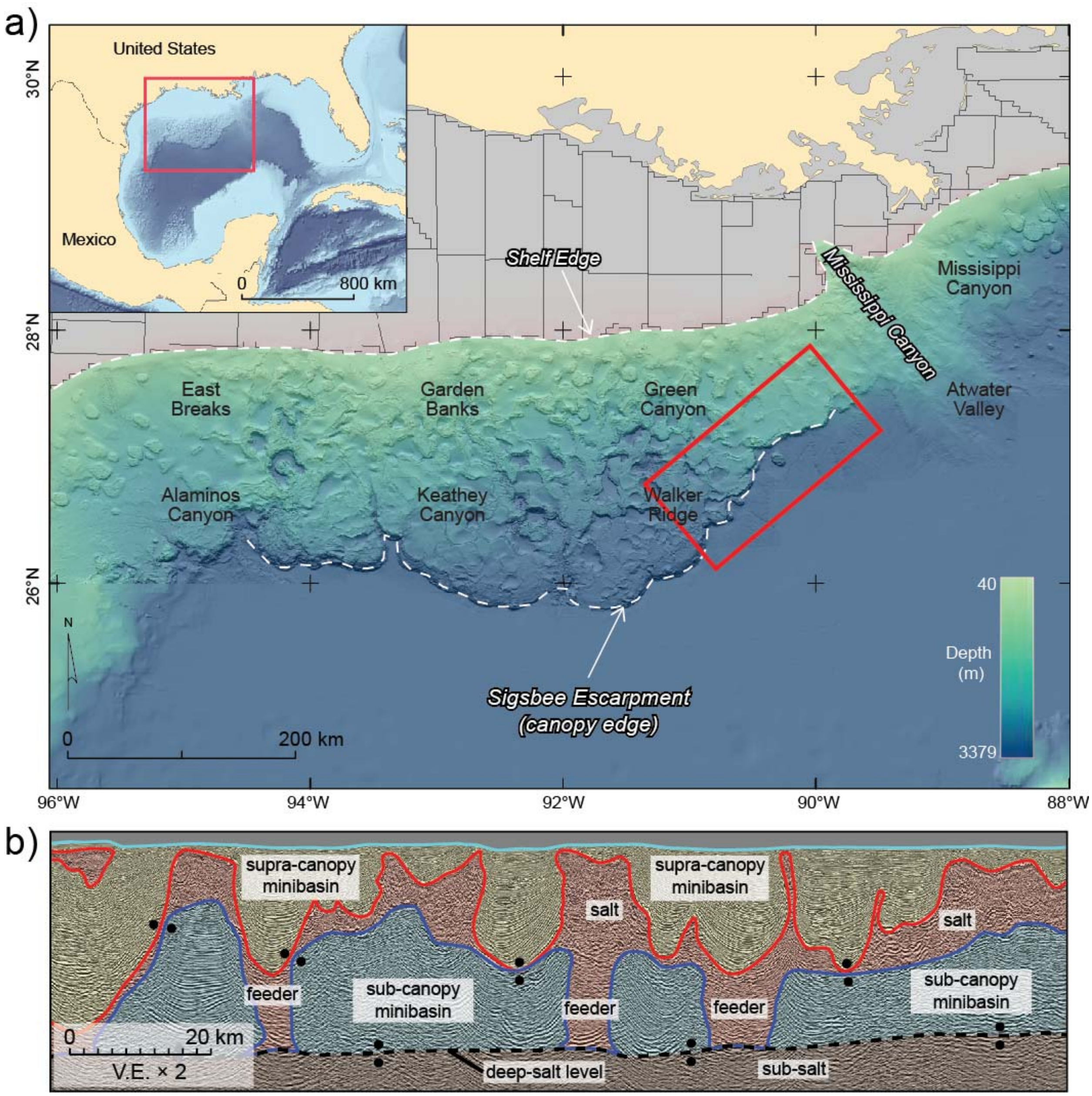

*Figure 2. **a)** Seafloor bathymetry map of the Northern Gulf of Mexico, where the study area is located (approximate location given by red rectangle). The Sigsbee Escarpment and the Shelf Edge, delimit the approximate extend of the Sigsbee canopy. Labels represent the main protraction areas of the northern Gulf of Mexico slope. Bathymetry map is created from a combination of data from the BOEM and NOAA. **b)** An interpreted seismic cross-section covering the study area illustrates the different structural elements present (from Fernandez et al., 2021). The section orientation is roughly along-strike of the slope. The top of salt horizon (in red) and the base-of-salt horizon (in dark blue) are relevant for the present study as represent the potential for minibasins to be obstructed. The feeders are the vertical salt conduits that allowed salt to move from the deep-salt level to the canopy level. Welding is indicated by paired black dots. Exact location of study area and seismic cross-section cannot be released due to commercial sensitivity of the seismic data.*

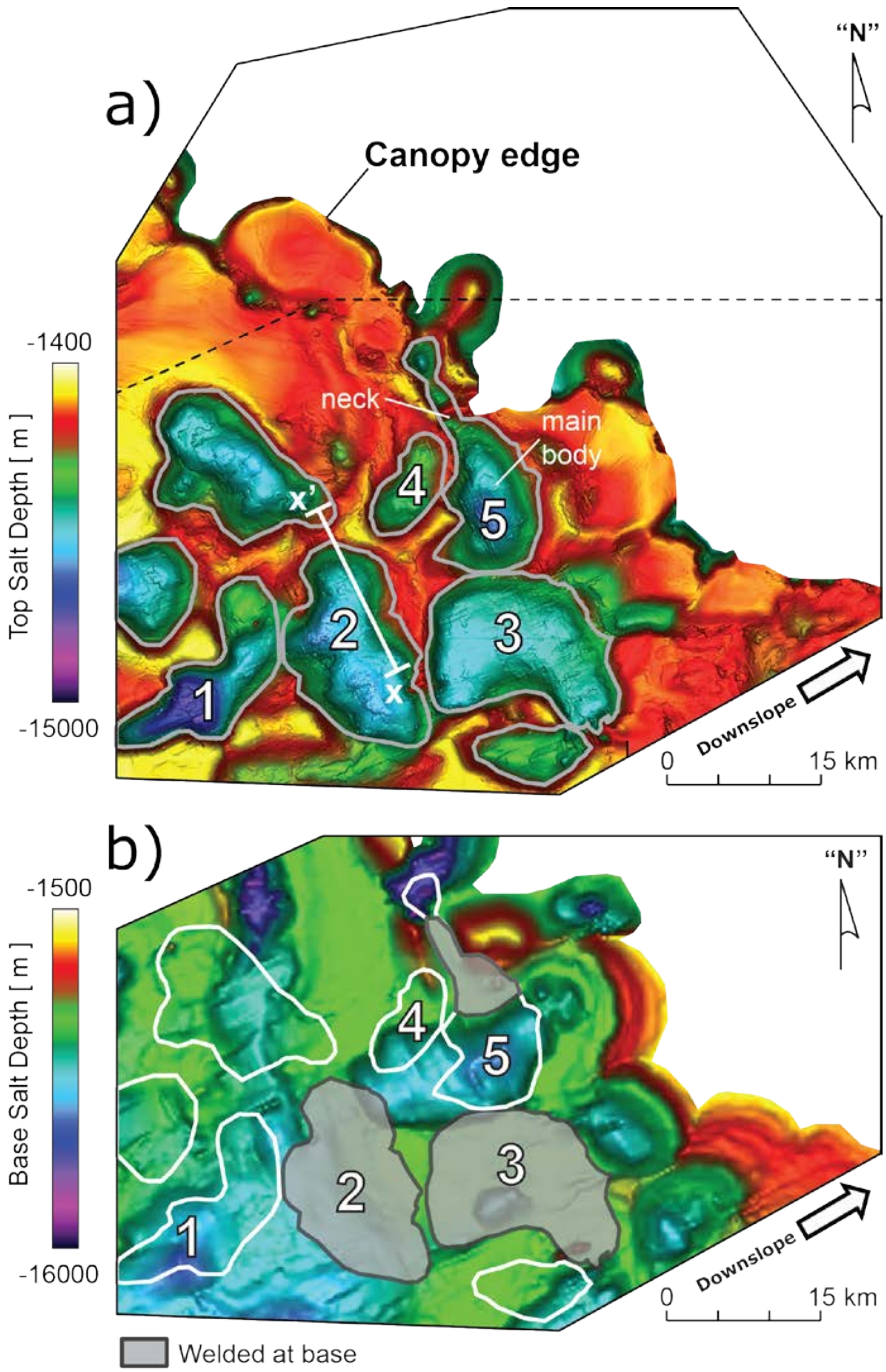

__Figure 3. a)__ Top salt structure map of the study area. The limit of the colored structure map represents the limit of the shallow salt, indicated here as the canopy edge. Uncolored areas correspond to the continental rise. Yellow-red colors indicate structurally high areas and represent salt diapirs, salt sheets and other salt structures. Purple-to-blue colors indicate the topographic lows in the map and represent the location of the supra-canopy minibasins. The minibasins relevant to this study are numbered from the most updip located one, number 1, to the most downdip located one, number 5. Cross section x-x' is shown in Fig. 4b. __b)__ Base salt structure map of study area. Minibasins welded to the base-of-salt topography are shaded in grey color. Minibasins 2 and 3 are welded, and the neck of minibasin 5 is welded.

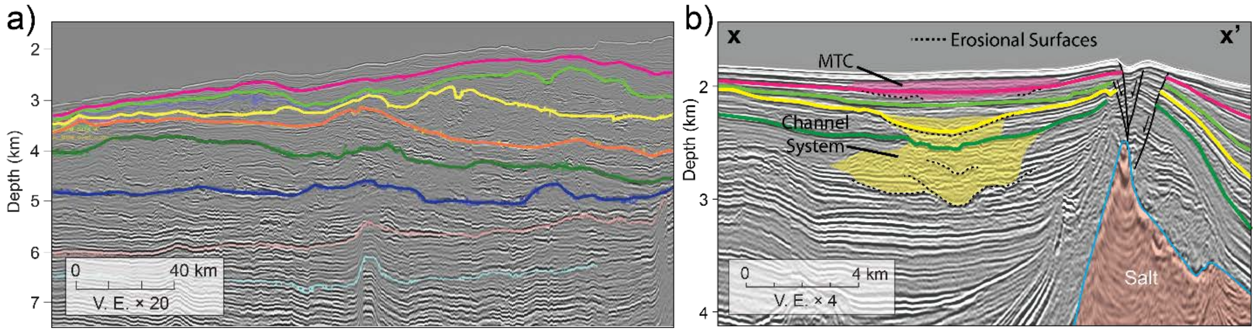

Figure 4. a) *Interpreted horizons outboard of the salt canopy, in the continental rise (uncolored areas in Figure 3). The horizons represent abandonment surfaces of long-lived depositional systems and represent regional events that can be tracked back to the supra-salt section above the salt canopy.* ***b)*** *Correlated horizons (dark-green, yellow, light-green and magenta) within the supra-canopy minibasins section (minibasin 2; see Figure 3a for location of section). Note the scale differences between a) and b).*

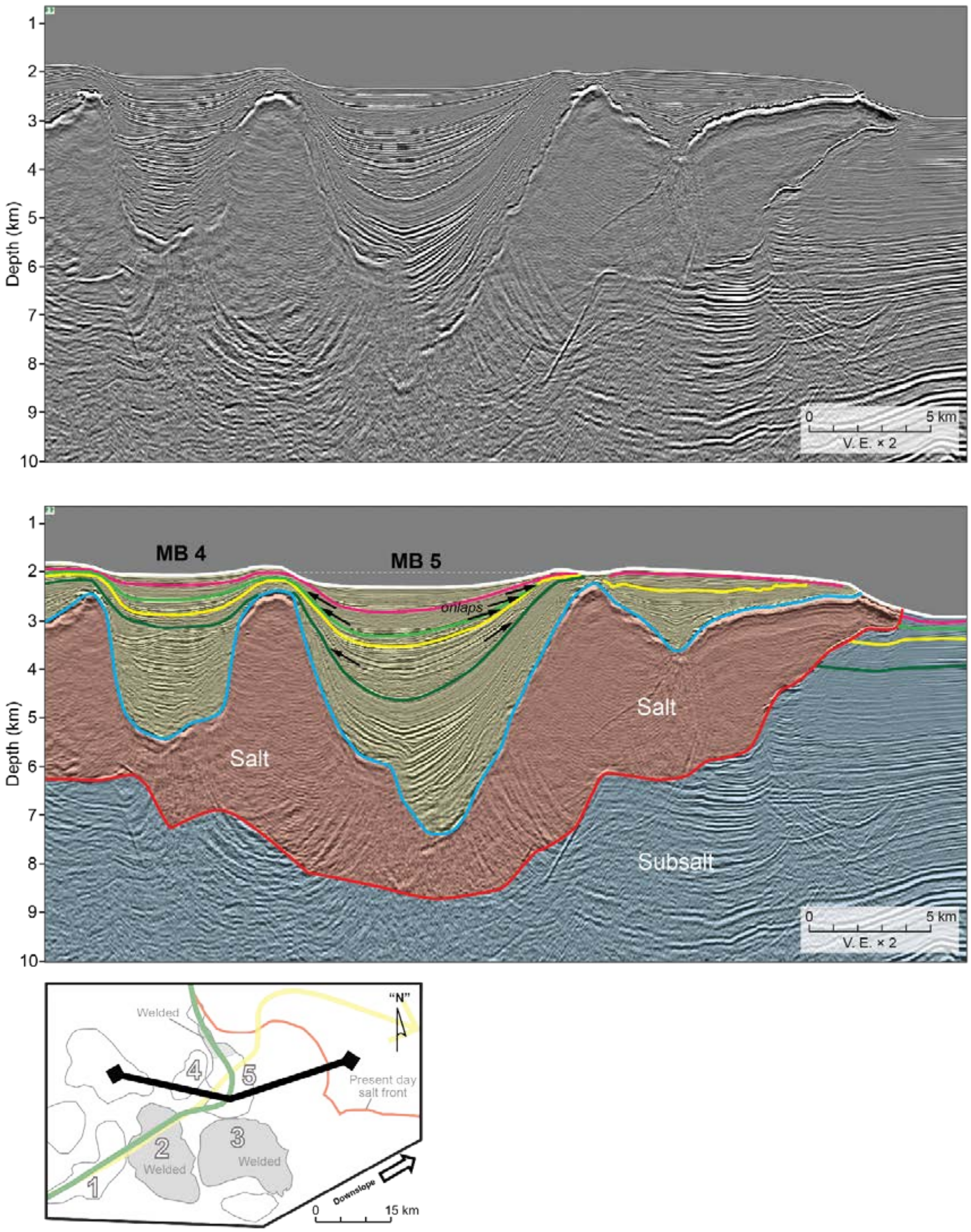

Figure 5. *Seismic cross section, across minibasin 4 and 5. Inset map shows the approximate location of the cross-section. The cross section shows that in this particular position, minibasin 5 is not welded at its base (there is still over 1 km of salt below). Minibasin 4 is also not welded. The seafloor topography above minibasin 5 also indicates that the minibasin 5 is still subsiding at present day in this particular area. Minibasins 4 and 5 are separated in this area by an intervening salt diapir.*

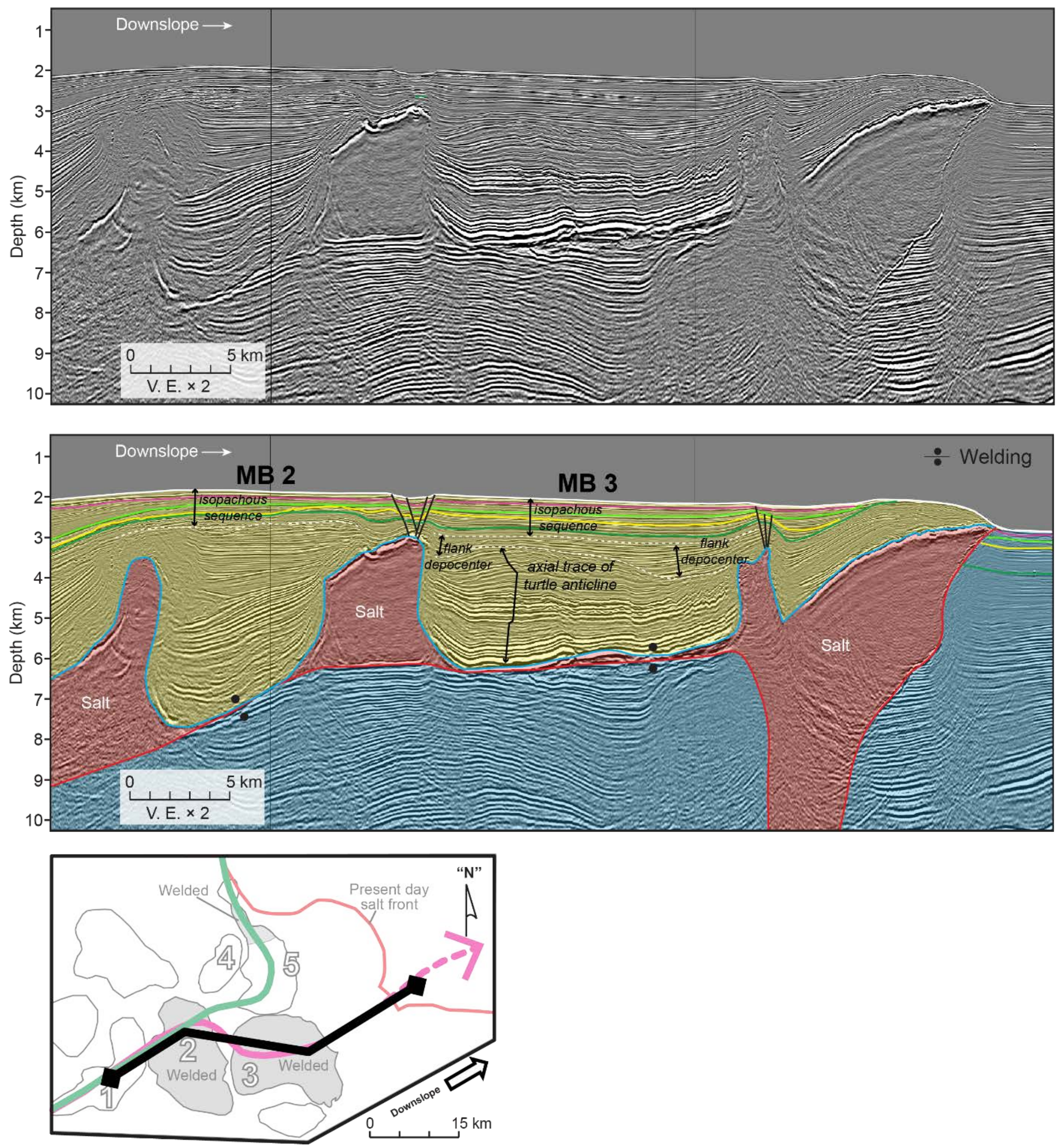

701

702 ***Figure 6.*** *Seismic section across minibasins 2 and 3. It shows that both minibasins are welded at its base. Interpretation of*
703 *constant thickness stratigraphic packages in both minibasins, indicates that welding occurred earlier than the dark- green*
704 *horizon shown in the section.*

705

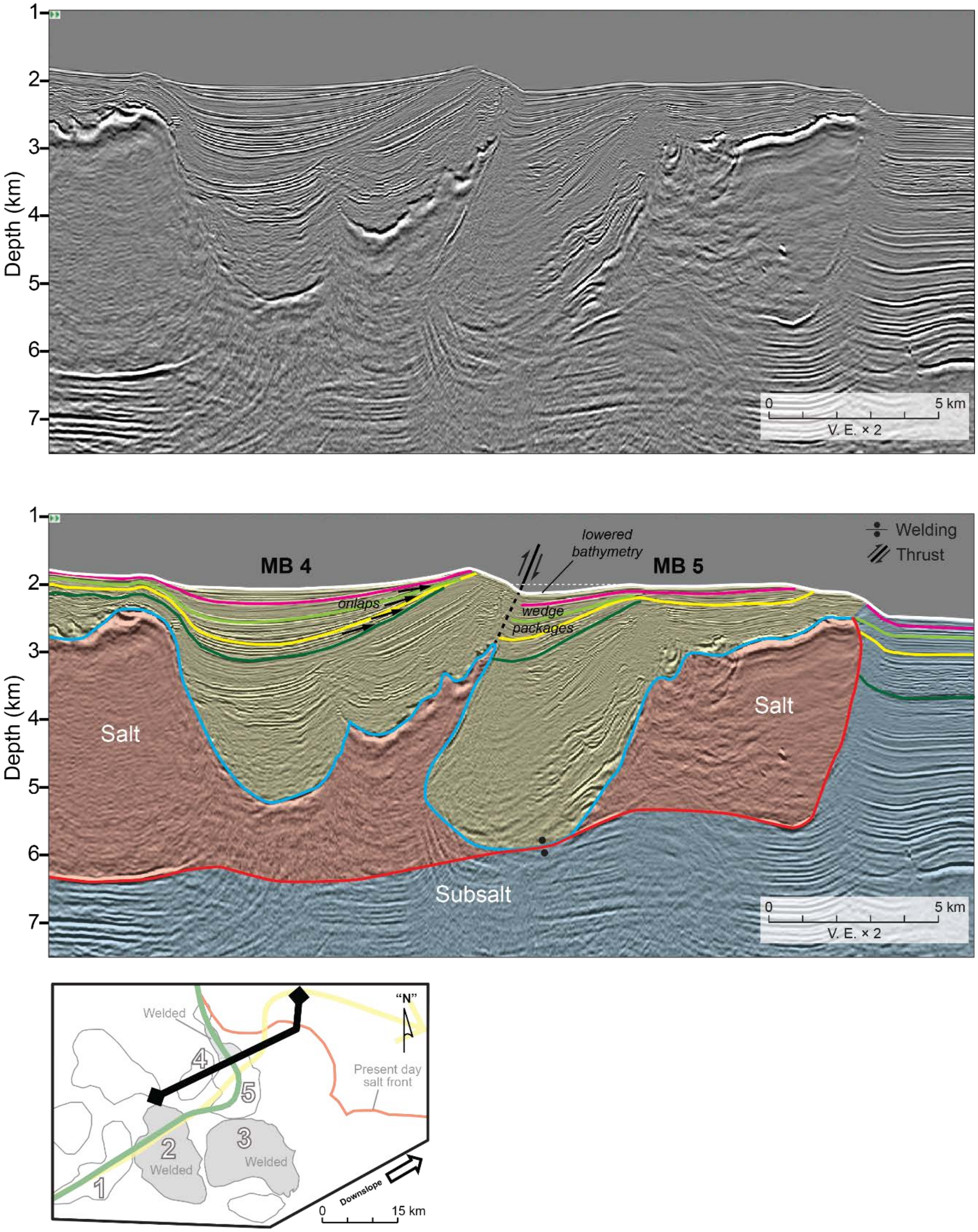

Figure 7. Seismic cross section, across minibasin 4 and 5. Inset map shows the approximate location of the cross-section, which is located further SW from the previous section. At this particular position, minibasin 5 is welded at its base and it is overthursted by minibasin 4 at its updip side.

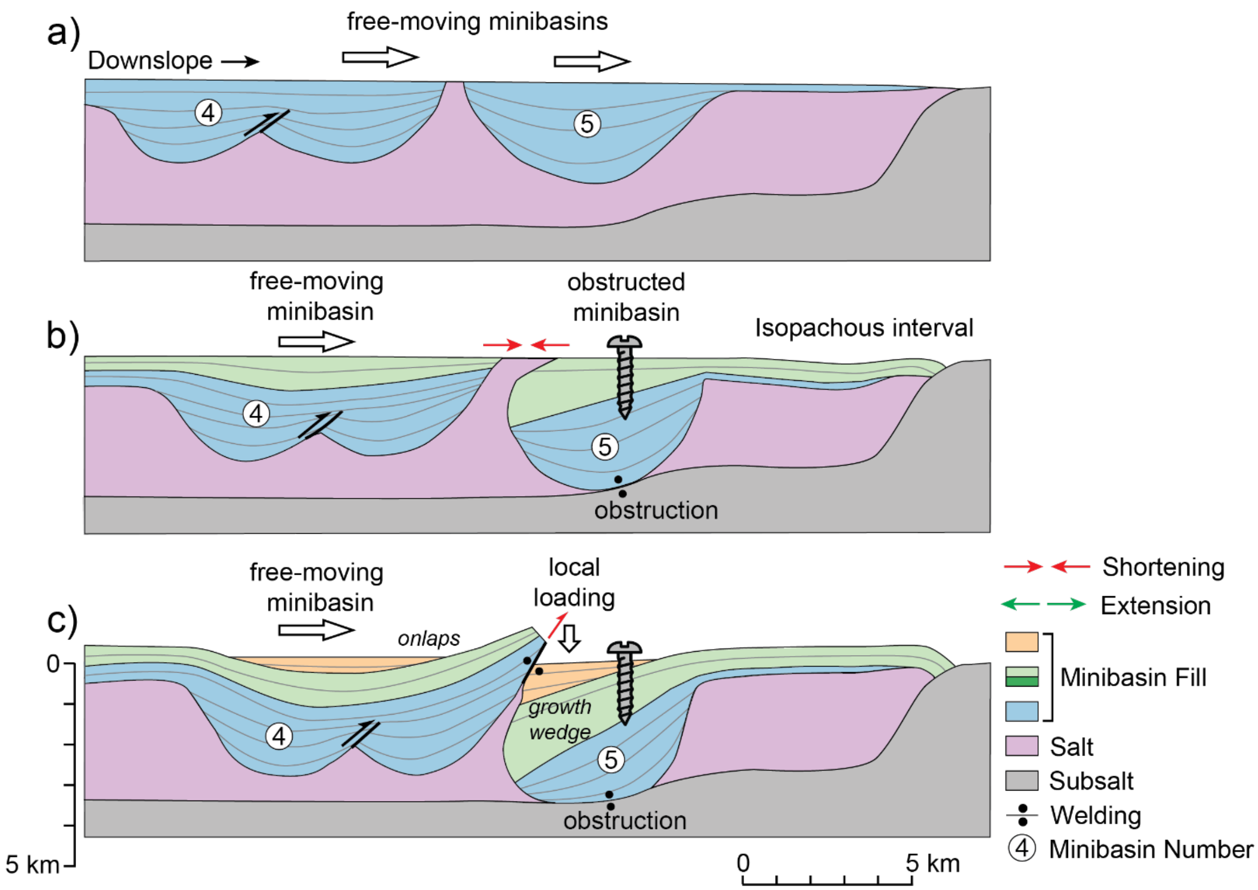

Figure 8. *Schematic sketch of the interpreted evolution of events that leads to minibasin 5 being overthursted by minibasin 4 updip.* ***a)*** *Initially none of the minibasins is welded at its base and they are being translated downslope with the flowing salt.* ***b)*** *As minibasins become thicker due to new sedimentation on top, minibasin 5 gets thick enough to weld against base-salt and gets obstructed from translation. Updip minibasin 4 is not welded and can continue translating downslope with the flowing salt and converge towards welded minibasin 5.* ***c)*** *As minibasin 4 keeps moving downslope, it collides with minibasin 5 and overthrusting it. The local loading due to the overthrusting pushes the updip edge of minibasin 5 downwards.*

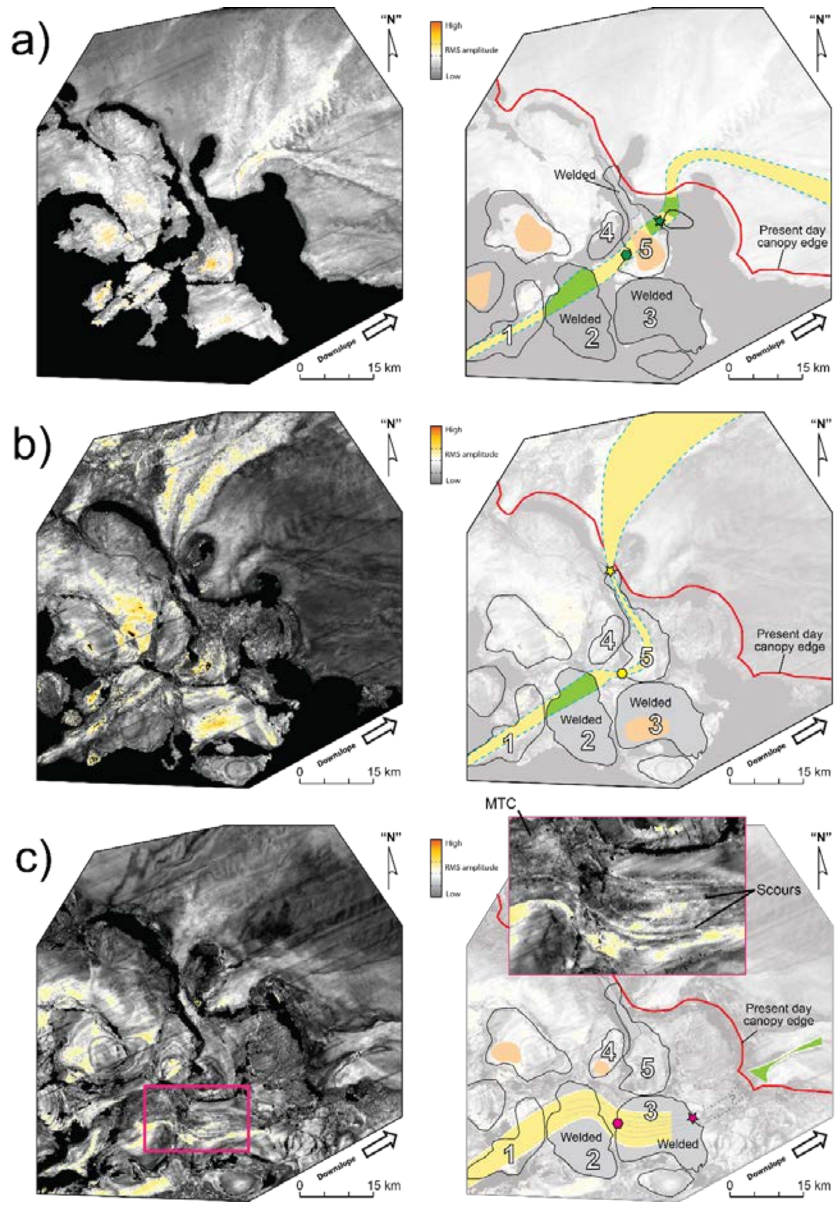

__Figure 9.__ Left panels: seismic attribute (RMS amplitude) extractions at 3 different regional horizons: dark-green (a), yellow (b) and magenta (c) (see also Figure 4). Right panels: interpretation of the main transport systems (yellow polygons) based on geomorphic features and the relative amplitude of the seismic attributes. Areas of sediment ponding (beige polygons) within minibasins and areas or erosional canyons or incision (green polygons) are indicated. __a)__ A submarine channel system that travels across minibasins 1, 2 and 5 is identified. The submarine channel system is interpreted to spill onto the continental rise through the downdip edge of minibasin 5 (dark-green star). __b)__ A submarine channel that travels across minibasins 1 and 2 following the same pathway as the previous channel system. It enters minibasin 5 at the same point as before (yellow hexagon), but after entering minibasin 5, instead of spilling following a straight path, the channel takes a left turn, travels across minibasin 5 (parallel to canopy edge) and spills into the continental rise at the northwest edge of minibasin 5 (yellow star). __c)__ A wide mass transport complex (rectangle area in shown as an inset detail on the right panel) travels across minibasins 1 and 2, but instead of travelling straight to minibasin 5, it takes a turn to the right, and deviates to continue traveling across minibasin 3 (magenta hexagon).

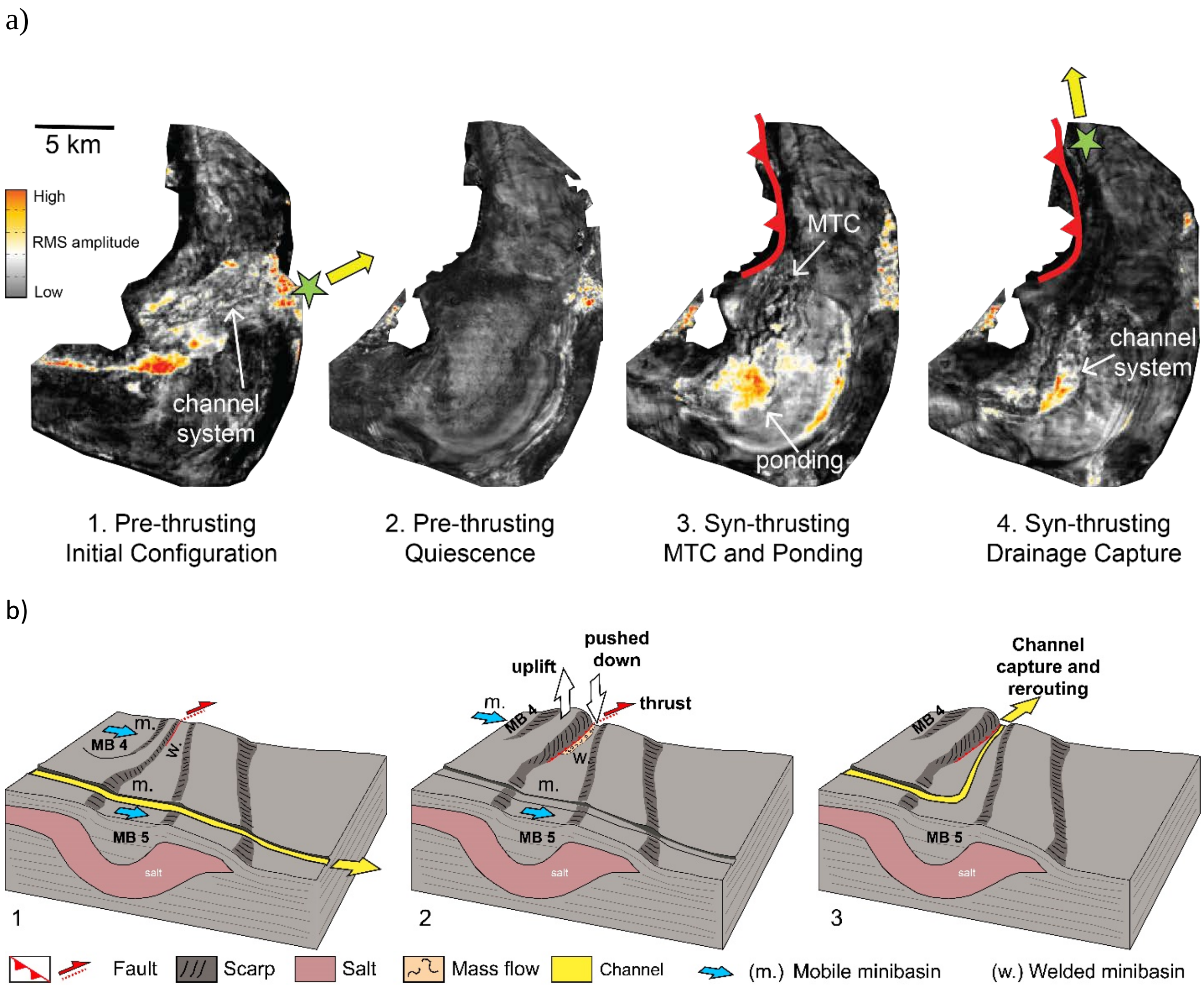

Figure 10. a) *Minibasin-scale high-resolution RMS extraction of four horizons that show the deflection of the submarine channel observed in minibasin 5. Stage 1 corresponds to the dark-green regional horizon, whereas Stage 4, corresponds to yellow regional horizon. Stages 2 and 3 are intermediate minibasin-scale horizons. Stars indicate spill-points consistent with observations in the regional RMS maps of Figure 8.* ***b)*** *Block diagram illustrating the drainage capture event caused by minibasin obstruction and overthrust and subsequent topographic lowering occurring in minibasin 5.*

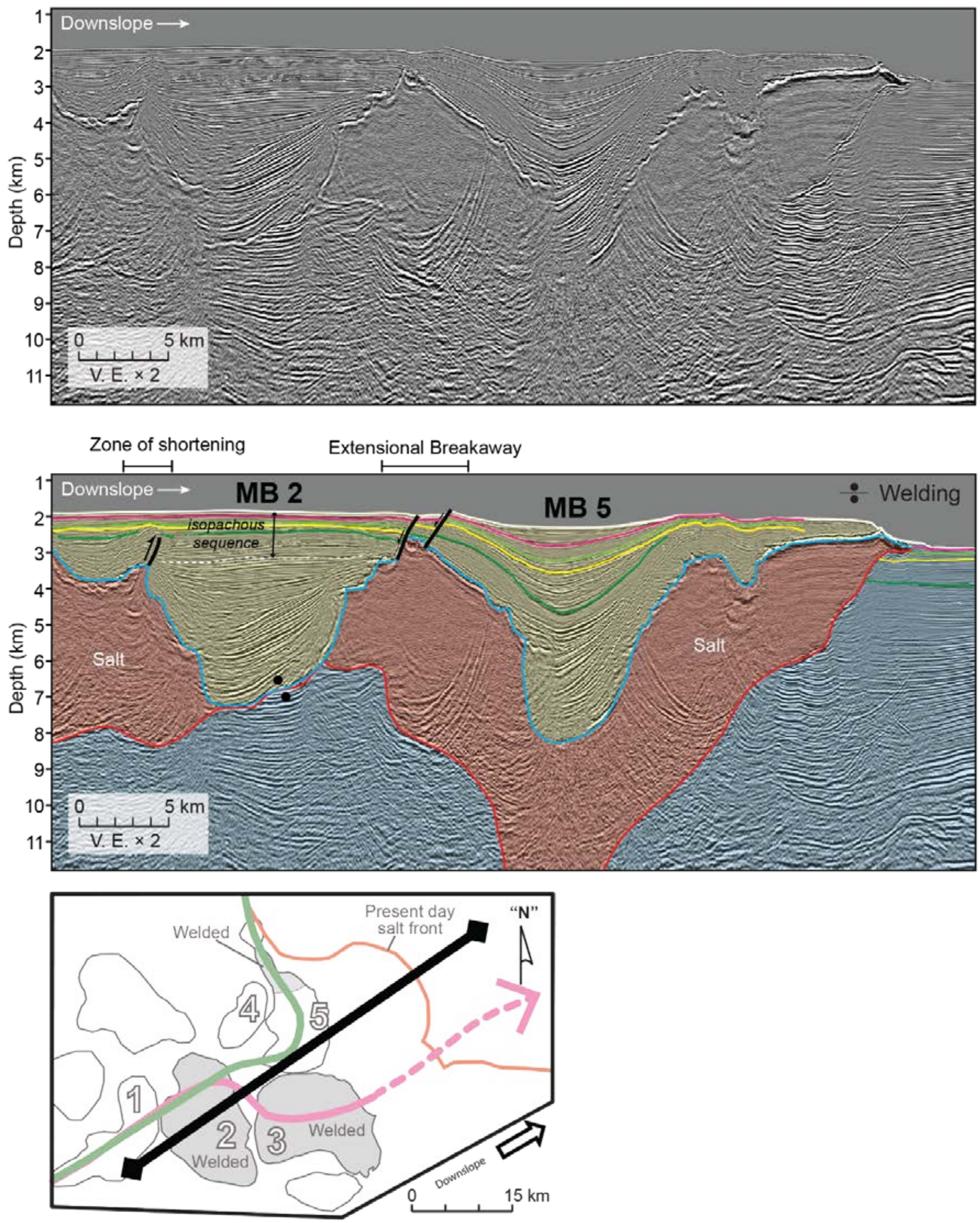

Figure 11. *Seismic cross section across minibasin 2 and 5. It shows the welded minibasin 2, and the unwelded minibasin 5. It also shows the faulted roof sedimentary sequence on top of the intervening salt structure between minibasins 2 and 5.*

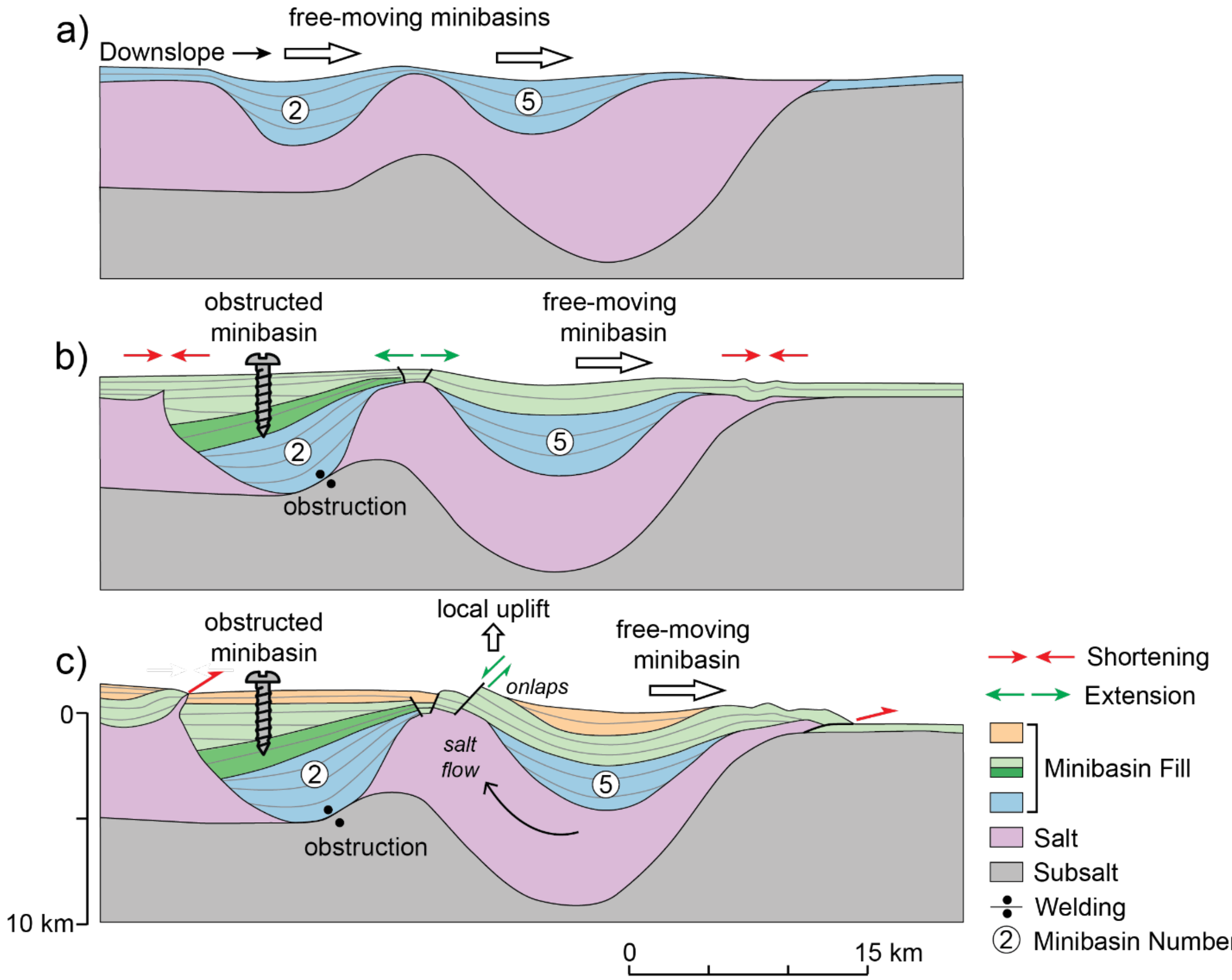

Figure 12. *Schematic sketch of the interpretation of events that lead to the faulting of the roof on top of diapir between minibasins 2 and 5.* ***a)*** *In an initial stage, none of the minibasins 2 and 5 are welded and they are moving downslope with the flowing salt.* ***b)*** *As they become thicker due to sedimentation on top, and because minibasin 2 is overlying an area of topographically higher base-of-salt, minibasin 2 welds and gets obstructed. Minibasin 5, which is located downdip of minibasin 2, continues translating downdip with the salt.* ***c)*** *As a result of the drifting of minibasin 5 away from minibasin 2, the roof on top of the diapir separating minibasins 2 and 5 gets stretched and several normal faults form. The footwall portion of the roof is locally uplifted, aided by inflowing salt from bellow minibasin 5.*

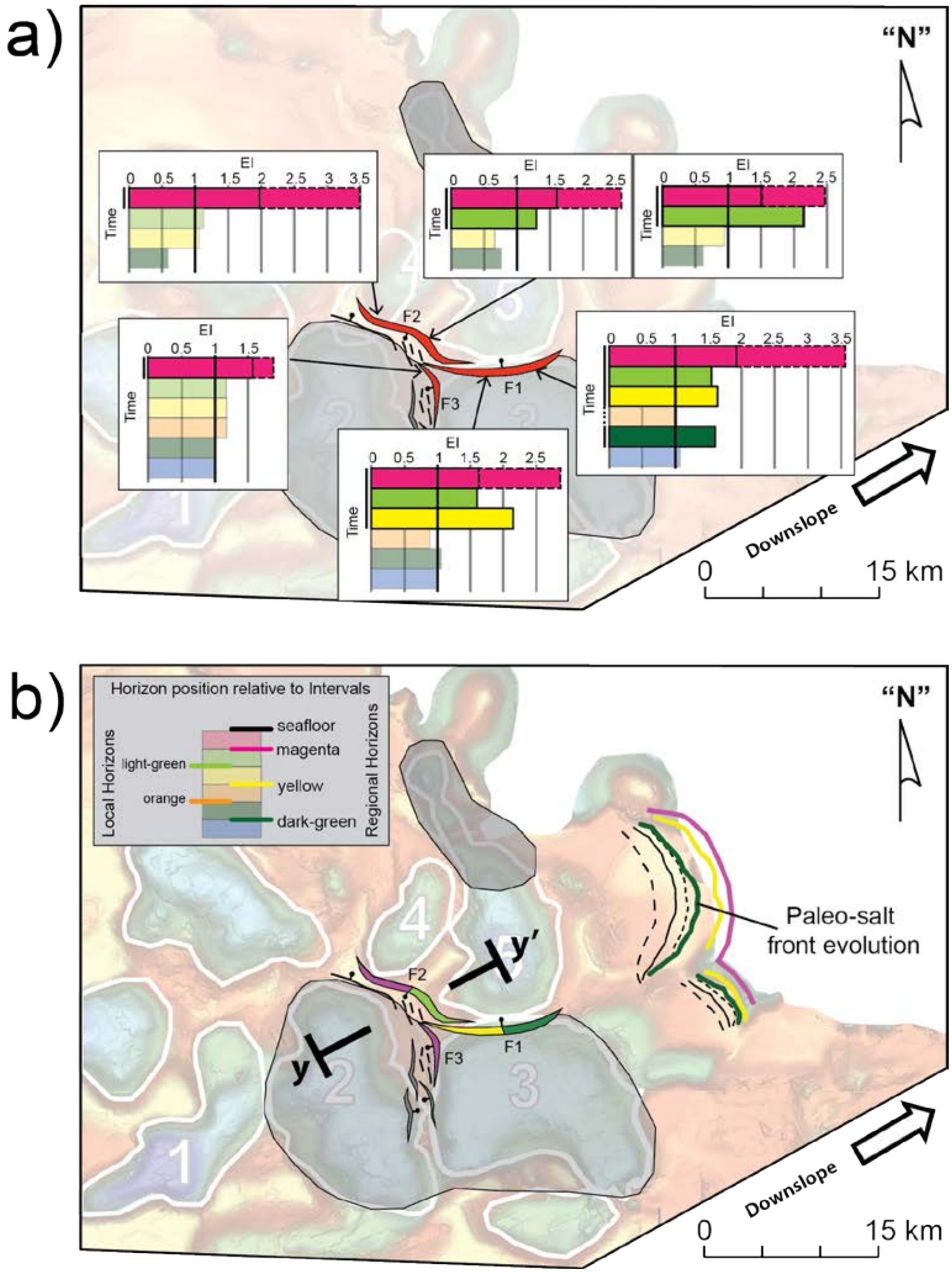

__Figure 13. a)__ Map view of the main fault segments between minibasins 2, 3,4 and 5. Each fault segment, F1, F2, and F3, has been analyzed using seismic cross sections to obtain an expansion index (EI), that indicates, fault activity at different time intervals, between the main mapped horizons (intervals are colored according to the horizon at their base). An expansion index EI>1, indicates that fault was most probably active during that time interval, if the thickness differences to both sides of the fault are interpreted as related to fault movement. __b)__ Map view of the fault segments and paleo-salt front evolution color coded according to their relative age (horizon interval). The EI analysis indicates that F1 segment activity started earlier, followed by F2 and F3. Fault displacement magnitude accumulated by F2, is matched by the displacement of the paleo-salt front evolution in front of minibasin 5 (as compared to the negligible displacing at the same time in front of minibasin 3). Section y-y' is shown in Fig. 14a.

a)

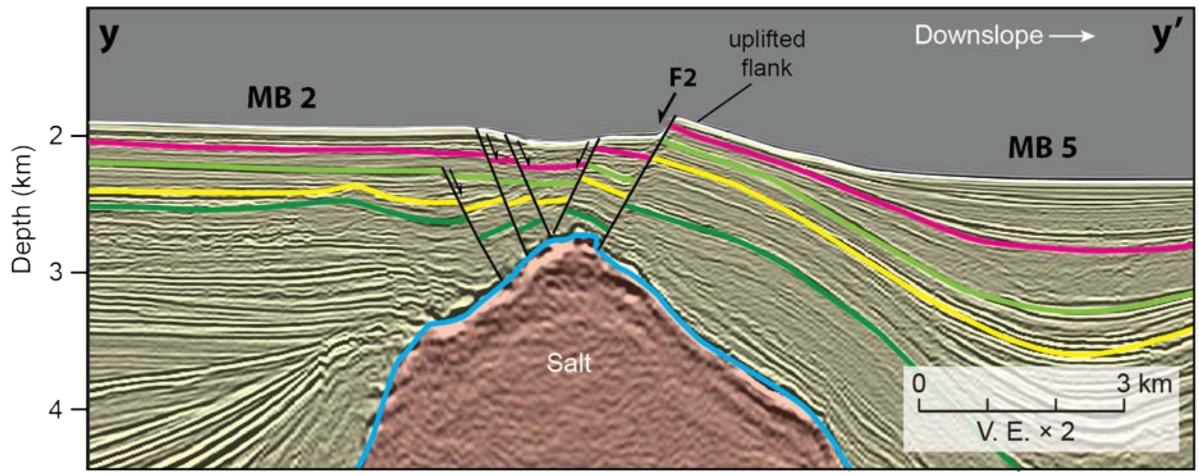

b)

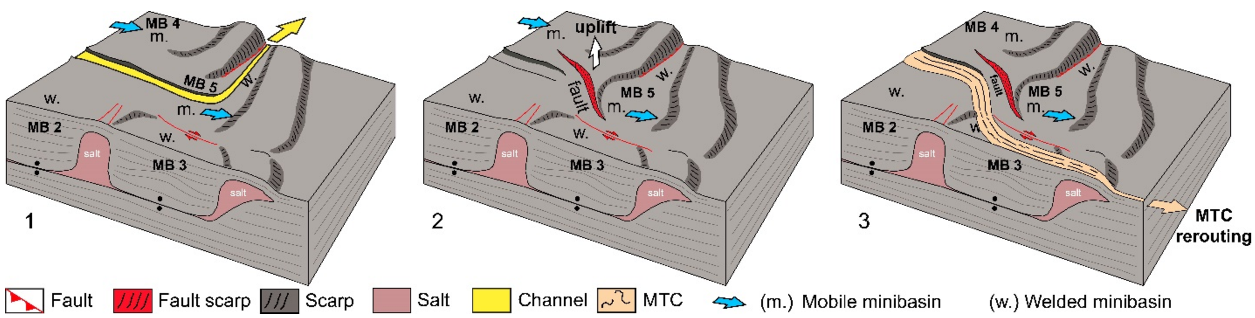

Figure 14. a) *Detail section of the fault system separating minibasin 2 (left) and minibasin 5 (right). The downslope footwall that corresponds to the flank of minibasin 5 shows a relative topographic elevation with respect to the base level of minibasin 2.* ***b)*** *Schematic block diagram that illustrates the minibasin obstruction associated extensional breakaway and its influence on the seafloor and on the sediment transport system configuration.*

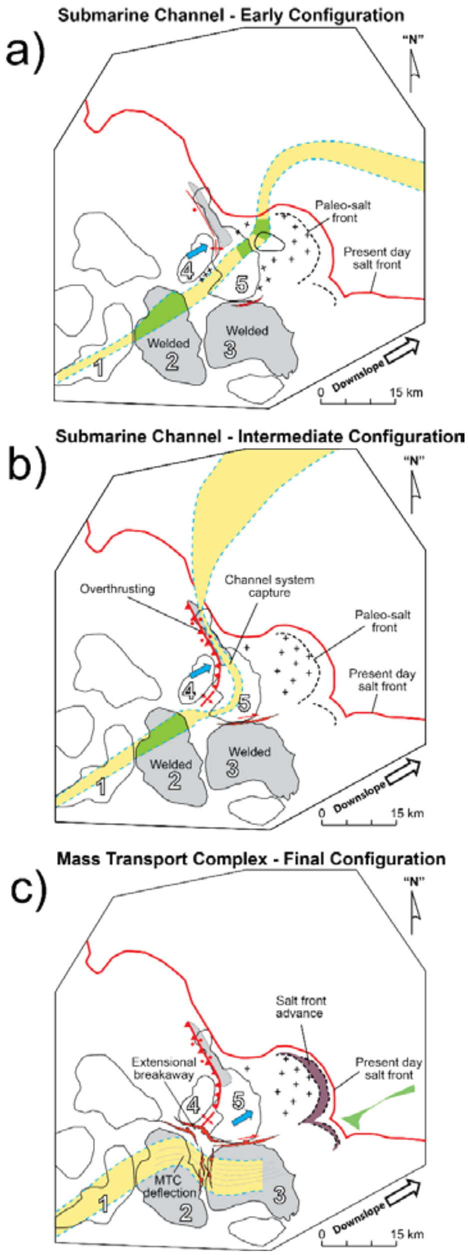

Figure 15. *Relation between the minibasin obstruction related events and their influence in the sediment transport systems interpreted in the RMS amplitude maps of Fig. 10a. Blue arrows indicate mobile minibasins.* ***a)*** *Initial configuration of the channel system. Shortening structures start developing between updip mobile minibasin 4 and partially obstructed downdip minibasin 5.* ***b)*** *Overthrusting of minibasin 4 onto partially obstructed minibasin 5, leads to the capture of the channel system and to the shift of the channel system pathway and final spill point onto the continental rise. Extensional (transtensional) faults start to develop between updip obstructed minibasin 3 and partially mobile downdip minibasin 5.* ***c)*** *An extensional breakaway form between updip obstructed minibasins 2-3 and mobile minibasins 4-5. The uplifted footwall creates a topographic barrier that deflects the MTC. The extensional breakaway is also reflected in higher differential advance of the salt canopy directly downdip of minibasin 5.*